

1 **The changing character of twenty-first century precipitation over the**
2 **western United States in the variable-resolution CESM**

3 Xingying Huang, * Paul A. Ullrich

4 *Department of Land, Air and Water Resources, University of California, Davis*

5 *Corresponding author address: Xingying Huang, Department of Land, Air and Water Resources,
6 University of California Davis, Davis, CA 95616.
7 E-mail: xyhuang@ucdavis.edu

ABSTRACT

8 The changing character of precipitation frequency and intensity in the west-
9 ern United States over the 21st century is investigated using an ensem-
10 ble of 26-year simulations with the variable-resolution Community Earth
11 System Model (VR-CESM) at a local grid resolution of $\sim 0.25^\circ$. Simula-
12 tions are forced using prescribed sea-surface temperatures, sea-ice extent and
13 greenhouse gas concentrations from the representative concentration pathway
14 (RCP) 8.5 scenario. VR-CESM is shown to be effective at accurately cap-
15 turing the spatial patterns of the historical precipitation climatology. In the
16 Intermountain West and Southwest U.S., we observe a statistically significant
17 increase in mean precipitation and rainy days through mid-century, although
18 this trend is tampered by end of century in response to a decrease in relative
19 humidity. In the Pacific Northwest, extreme precipitation events are observed
20 to increase significantly as a result of increased cool season integrated vapor
21 transport. In particular, extreme precipitation in this region appears to increase
22 more rapidly than would be predicted by the Clausius-Clapeyron relationship.
23 No clear climate signal emerges in mean precipitation or for extremes in Cali-
24 fornia, where the precipitation climatology is subject to large interannual vari-
25 ability that is tied more closely to ENSO. Results are discussed in the context
26 of the existing literature on precipitation extremes in the western U.S.

27 **1. Introduction**

28 There is substantial and growing interest in understanding the character of precipitation within
29 a changing climate, motivated largely by its pronounced impacts on water availability and flood
30 management in both human and natural systems (Hegerl et al. 2004; Kharin et al. 2007; Scoc-
31 cimarro et al. 2013). Among past studies addressing precipitation, extremes have been a major
32 focus, particularly drought and flood events (Seneviratne et al. 2012). Overall, it is widely agreed
33 that although atmospheric water vapor concentration is increasing, the impacts of a changing cli-
34 mate on the character of precipitation is far more complicated. Extreme precipitation events are
35 particularly nuanced: Our best projections suggest that extreme precipitation events will intensify
36 even in regions where mean precipitation decreases (Tebaldi et al. 2006; Kharin et al. 2007).

37 Future climate projections, particularly those addressing the frequency and intensity of rare
38 events, are inevitably subject to large uncertainties. Nonetheless, climate models have been inval-
39 able tools for developing insight into this problem (Easterling et al. 2000). In particular, global
40 climate models (GCMs) have often been used to investigate changes in the mean, variability and
41 extremes of climate, as forced with predicted greenhouse gas (GHGs) concentrations and aerosol
42 emissions (Meehl et al. 2006). Although several past studies have investigated climate extremes at
43 the global scale (Seneviratne et al. 2012), studies addressing extremes at local and regional scales
44 are less common. It is well understood how increased GHG concentrations have contributed to
45 the observed intensification of heavy precipitation events over the tropical ocean (Allan and Soden
46 2008) and the majority of Northern Hemisphere overland areas (Min et al. 2011), but changes are
47 much more poorly understood at regional scales where meteorological variability is large (Tren-
48 berth 2011). As a consequence of this variability, confidence in the assessment of regional extreme
49 precipitation changes requires both high spatial resolution and a long integration period, both of

50 which can make the computational cost untenable for global simulations. This issue of insufficient
51 regional-scale climate information has been a major outstanding problem in climate science, as
52 stakeholders and water managers typically require fine-scale information on climate impacts in
53 order to effectively develop adaptation and mitigation strategies.

54 Dynamical downscaling with regional climate models (RCMs) has been one of the few tools
55 available to ascertain the frequency, intensity, and duration of extreme events at the needed scales.
56 By only simulating a limited regional domain, RCMs better capture fine-scale dynamical features
57 with high horizontal resolution (Bell et al. 2004; Frei et al. 2006; Rauscher et al. 2010; Wehner
58 2013). Higher resolution enables more accurate simulation of precipitation extremes, which are
59 driven by circulation patterns, cloudiness, land use, land/water contrast, snowpack and topography
60 (Leung et al. 2003a; Diffenbaugh et al. 2005; Salathé Jr et al. 2008; Wehner et al. 2010). For exam-
61 ple, Leung et al. (2003b) showed that the higher-resolution RCMs yield more realistic precipitation
62 patterns and produce more frequent heavy precipitation over the western U.S. (WUS), consistent
63 with observations. Diffenbaugh et al. (2005) studied both extreme temperature and precipitation
64 events over the contiguous United States using a RCM configured at 25 km horizontal resolu-
65 tion, and demonstrated that fine-scale processes were critical for accurate assessment of local- and
66 regional-scale climate change vulnerability. Salathé Jr et al. (2008) found significant differences in
67 trends for temperature and precipitation over the Pacific Northwest using a high-resolution RCM
68 for future climate simulations. And Ashfaq et al. (2016) observed a 7.4% increase in precipitation
69 from extremes over the contiguous U.S. from simulations with RegCM4 driven by CMIP5 global
70 data.

71 Despite their success, RCMs also have known issues associated with inconsistency between
72 the lateral forcing data and the driven RCM. The menu of physical parameterizations and tuning
73 parameters typically available to RCMs can also lead to over-tuning of the model for a partic-

⁷⁴ ular geographic region or climatological field (McDonald 2003; Laprise et al. 2008; Mesinger
⁷⁵ and Veljovic 2013). Consequently, there has been growing interest in variable-resolution enabled
⁷⁶ GCMs (VRGCMs) to improve regional climate simulations. Unlike RCMs, which require GCM
⁷⁷ data to drive the simulation at lateral boundaries, VRGCMs use a unified model with coarse global
⁷⁸ resolution and enhanced resolution over a specific study region (Staniforth and Mitchell 1978;
⁷⁹ Fox-Rabinovitz et al. 1997). VRGCMs have demonstrated competitive ability for regional climate
⁸⁰ studies at a reduced computational cost, particular when compared to uniform-resolution GCMs
⁸¹ (Fox-Rabinovitz et al. 2006; Rauscher et al. 2013).

⁸² In this paper, we utilize the recently developed variable-resolution option in the Community
⁸³ Earth System Model (VR-CESM). VR-CESM is based on the CESM (and its predecessor, the
⁸⁴ Community Climate System Model (CCSM)), a family of models that have been used for decades
⁸⁵ to study the global climate (Neale et al. 2010a; Hurrell et al. 2013). The overall performance
⁸⁶ of VR-CESM for modeling regional climate in the California and Nevada is detailed in Huang
⁸⁷ et al. (2016), where it was argued that VR-CESM has competitive biases in comparison to the
⁸⁸ Weather Research and Forecasting (WRF) model (a traditional RCM) and the uniform-resolution
⁸⁹ CESM, when evaluating against high-quality observations and reanalysis. VR-CESM has been
⁹⁰ used in a number of studies to simulate fine-scale atmospheric processes (Zarzycki et al. 2014,
⁹¹ 2015; Rhoades et al. 2015; Huang and Ullrich 2016; Rhoades et al. 2016).

⁹² This study focuses on changes in the character of precipitation over the 21st century within the
⁹³ WUS, as predicted from long-term ensemble runs conducted with VR-CESM with a local grid
⁹⁴ resolution of $\sim 0.25^\circ$. The WUS is known to be particularly vulnerable to hydrological extremes,
⁹⁵ particularly floods and droughts (Leung et al. 2003b; Caldwell 2010), and hosts a variety of local
⁹⁶ features and microclimates associated with its rough and varied topography. Simulations of the
⁹⁷ future climate are performed in accordance with the representative concentration pathway (RCP)

8.5 scenario, which describes a “business-as-usual” projection for GHGs (Riahi et al. 2011). In this study we focus singularly on the RCP 8.5 scenario because its mid-century results are similar to a more optimistic RCP2.6 scenario end-of-century. Simulations are further conducted in accordance with the Atmospheric Model Intercomparison Project (AMIP) protocol (Gates 1992), a widely-used approach for climate model diagnosis, validation and intercomparison that imposes global sea surface temperatures (SSTs) and sea ice. It is well-known that correctly simulating changes to the spatial pattern of SSTs in state-of-the-art coupled GCMs remains a significant challenge (Joseph and Nigam 2006; Stevenson 2012; Jha et al. 2014; Taschetto et al. 2014). However, by constraining atmospheric boundary conditions at the sea surface, we avoid model biases that are known to exist in the fully coupled configuration (Grodsby et al. 2012; Small et al. 2014) but accept potential uncertainties associated with our choice of SSTs.

Changes in the character of precipitation, in terms of frequency and intensity, have been assessed in our study from recent history through the end of the 21st century. A comprehensive set of indices for precipitation extremes have been evaluated from the ensemble simulations over the 26-year periods corresponding to historical (1980-2005), mid-century (2025-2050) and end-of-century (2075-2100). Spatial inhomogeneity in local geography and temperature are observed to result in similarly inhomogeneous impacts on the precipitation field. Teleconnections (specifically the El Niño-Southern Oscillation, ENSO) are also observed to have a pronounced impact on precipitation features. Since only one SST dataset was used for this study, we note that our projections are conditioned on a particular future character of ENSO. This is a potentially large source of uncertainty, as at present there is no clear consensus on how ENSO may behave under a warming climate (Fedorov and Philander 2000; Latif and Keenlyside 2009; Guilyardi et al. 2009; Collins et al. 2010; DiNezio et al. 2012), and strengthening or weakening of this pattern will have clear consequences for our results (as discussed in section 6d).

122 This work builds on a number of previous studies that have explored the projected future change
123 in WUS precipitation. For example, Kim (2005) applied downscaled climate change signals to se-
124 lected indicators, and concluded that global warming induced by increased CO₂ is likely to drive
125 increases in extreme hydrologic events in the WUS. Duffy et al. (2006) found that changes to
126 mean precipitation predicted by the RCMs are not statistically significant compared to interannual
127 variability in many regions over WUS, although there is little consistency among the different
128 RCMs as to responses in precipitation to increased GHGs. Gao et al. (2015) pointed out a poten-
129 tially large increase in atmospheric river events by the end of the 21st century under the RCP8.5
130 scenario, with implications for large-scale and heavy precipitation events along the Pacific coast.

131 This paper is structured as follows. Section 2 describes the model setup. Section 3 describes
132 the methodology and reference datasets employed. An assessment of the ability of the model to
133 capture the climatology of the WUS is given in section 4. Results from the future mean climato-
134 logical trend and projected changes to precipitation indices are in section 6. Section 7 summarizes
135 the main points of the study along with further discussion.

136 2. Model Setup

137 CESM is a state-of-the-art Earth modeling framework, consisting of coupled atmosphere, ocean,
138 land and sea ice models (Neale et al. 2010b; Hurrell et al. 2013). In this study, the Community At-
139 mosphere Model version 5 (CAM5) (Neale et al. 2010b) and the Community Land Model version
140 4.0 (Oleson et al. 2010) are used. CAM5 is configured with the Spectral Element (SE) dynamical
141 core, which is known for its conservation properties, accuracy and parallel scalability (Dennis et al.
142 2011; Taylor 2011) and incorporates the variable-resolution option (Zarzycki et al. 2014). CLM
143 is employed in the *unigrid* configuration, which allows the land model and atmospheric model to
144 utilize the same model grid so eliminates the need for interpolation. SSTs and sea ice, which are

¹⁴⁵ used to compute ocean-atmosphere fluxes, are prescribed in accordance with the AMIP protocol
¹⁴⁶ (Gates 1992). The variable-resolution mesh used for this study is depicted in Figure 1, in accord
¹⁴⁷ with our past studies (Rhoades et al. 2015; Huang et al. 2016; Huang and Ullrich 2016; Rhoades
¹⁴⁸ et al. 2016).

¹⁴⁹ Simulations have been performed for the historical period (1979-2005, hereafter referred to as
¹⁵⁰ hist) and for two future periods: 2024-2050 (hereafter referred to as mid) and 2074-2100 (hereafter
¹⁵¹ referred to as end). Daily output are recorded for each period on the native SE grid and then
¹⁵² remapped to a regional latitude-longitude mesh (Ullrich and Taylor 2015; Ullrich et al. 2016). For
¹⁵³ purposes of analysis, the first year of each time period was discarded as a spin-up period to allow
¹⁵⁴ adequate time for the initialized land and atmosphere to equilibrate. The 26-year duration was
¹⁵⁵ chosen to provide an adequate sampling of annual variability for each time phase. As mentioned
¹⁵⁶ earlier, GHG concentrations are set based on RCP8.5. Historical SSTs and sea ice are prescribed
¹⁵⁷ at 1° resolution, as described by Hurrell et al. (2008). SSTs and sea ice for each future period are
¹⁵⁸ developed from fully-coupled RCP 8.5 climate simulations with bias correction applied (Cecile
¹⁵⁹ Hannay, personal communication). Annually-updated land surface datasets, which prescribe land-
¹⁶⁰ use characteristics, are interpolated from 0.5° to the land model grid.

¹⁶¹ Ensemble runs are needed to ensure that the sample adequately accounts for climate variability,
¹⁶² especially for statistics associated with climatological extremes. However, the exact number of
¹⁶³ ensemble members required is heavily dependent on the variability of the particular metric being
¹⁶⁴ examined, and so no standard ensemble criteria exists. Deser et al. (2012b) suggest that around
¹⁶⁵ 3 ensemble runs are required to detect a significant epoch difference for JJA (June-July-August)
¹⁶⁶ surface temperatures, whereas 10 to 30 ensemble members are needed for that for DJF (Dec.-Jan.-
¹⁶⁷ Feb.) precipitation. In our study, the use of prescribed SSTs does reduce the intrinsic variability

¹⁶⁸ of the climate system (see supplement), and so we found reasonably converged results with two
¹⁶⁹ ensemble members for the historical period and four ensemble members for each future period.

¹⁷⁰ **3. Methodology**

¹⁷¹ *a. Precipitation indices*

¹⁷² Standard indices have been employed to characterize precipitation (Tebaldi et al. 2006; Zhang
¹⁷³ et al. 2011; Sillmann et al. 2013). In order to choose a comprehensive (but minimal) set that
¹⁷⁴ are informative to stakeholders and water managers, indices from throughout the literature were
¹⁷⁵ compiled. The indices examined include those defined by the Expert Team on Climate Change
¹⁷⁶ Detection and Indices (ETCCDI) (Karl et al. 1999) that are featured in earlier studies (Dulière
¹⁷⁷ et al. 2011; Sillmann et al. 2013; Diffenbaugh et al. 2005; Singh et al. 2013) and others such as
¹⁷⁸ return levels, dry spell and wet spell characteristics defined by either percentiles or by selected
¹⁷⁹ thresholds. As a result, the indices we have chosen for this study attempt to provide a relatively
¹⁸⁰ comprehensive characterization of precipitation, and are summarized in Table 1. Indices related to
¹⁸¹ dry spells of variable duration have been investigated in this study, but only exhibited significant
¹⁸² differences for extremely short (< 5 day) dry spells and so are not included in our results.

¹⁸³ *b. Impacts of ENSO*

¹⁸⁴ The impact of ENSO on precipitation is emphasized in our study due to its influence on precipi-
¹⁸⁵ tation over a majority of our study area, particularly the southwest U.S. (Cayan et al. 1999; Zhang
¹⁸⁶ et al. 2010; Deser et al. 2012a; Yoon et al. 2015). The phase of ENSO (*i.e.* El Niño and La Niña)
¹⁸⁷ is identified each year using the Oceanic Niño Index (ONI), defined as the 3-month running means
¹⁸⁸ of SST anomalies in the Niño 3.4 region (covering 5N-5S, 120-170W based on NOAA (2013)).
¹⁸⁹ An El Niño or La Niña episode is said to occur when the ONI exceeds +0.5 or -0.5 for at least five

190 consecutive months for a water year (i.e. from July to June) (NOAA 2013) (see the supplement).

191 In order to adjust for the trend in the SST field associated with climate change, the anomaly is
192 computed against the detrended mean SSTs from the periods 1971-2000, 2020-2050 and 2070-
193 2100 for hist, mid and end respectively, using the aforementioned observed and predicted SST
194 datasets. As argued by Kao and Yu (2009), it may be desirable to use an extended Niño 3.4 region
195 to determine the phase of ENSO – however, when employing SST anomalies integrated over the
196 region 105-170W, we observed no significant impact on ONI statistics.

197 *c. Assessing statistical significance*

198 Student's t-test has been used to determine whether or not two datasets at each grid point are sta-
199 tistically equivalent, if the sample population can be adequately described by a normal distribution.
200 The normality of a dataset is assessed under the Anderson-Darling test. When the sample popu-
201 lations do not approximately follow a normal distribution, Mann-Whitney-Wilcoxon (MWW) test
202 is employed in lieu of the t-test. All tests are evaluated at the 0.05 (α) significance level. When
203 comparing different time periods, statistical tests are conducted by treating all years from all en-
204 semble members as independent samples (26×2 sample years for hist and 26×4 sample years
205 for mid and end).

206 (add description of the supplement like what are included; see the sst_enso.pdf, mask the land
207 (over land, it should be the surface temperature.))

208 *d. Reference datasets*

209 Gridded observational datasets and reanalysis of the highest available quality, with comparable
210 horizontal resolutions to our VR-CESM simulations, are used for assessing the simulation quality.

211 Multiple reference datasets are necessary due to the underlying uncertainty in the precipitation
212 field. The three datasets employed are as follows:

213 **UW Gridded Data:** The 0.125° UW daily gridded meteorological data is obtained from
214 the Surface Water Modeling group at the University of Washington, covering the period
215 1949-2010 (Maurer et al. 2002; Hamlet and Lettenmaier 2005). The UW dataset imposes
216 topographic corrections by forcing the long-term average precipitation to match that of the
217 Parameter-elevation Regressions on Independent Slopes Model (PRISM) dataset.

218 **National Centers for Environmental Prediction (NCEP) Climate Prediction Center**
219 **(CPC):** The 0.25° CPC daily dataset provides gauge-based analysis of daily precipitation cov-
220 ering the period 1948-2006. It is a unified precipitation product that covers the Conterminous
221 United States and amalgamates a number of data sources at CPC via optimal interpolation
222 objective analysis.

223 **North American Regional Reanalysis (NARR):** The ~ 32 km NCEP NARR reanalysis pro-
224 vides 3-hourly precipitation snapshots, obtained by dynamical downscaling over North Amer-
225 ica and covering the period 1979-present (Mesinger et al. 2006).

226 **4. Assessment of Precipitation Character in VR-CESM**

227 Before proceeding, we assess the ability of VR-CESM to represent the character of precipitation
228 over the WUS. The indices defined in Table 1 are depicted in Figures 2, 3 and 4 for VR-CESM
229 and each of the reference datasets over the historical period (1980-2005). We assume equal con-
230 fidence in each of the reference datasets, and use Student's t-test (with UW, CPC and NARR as
231 the three statistical samples) to identify regions where VR-CESM deviates significantly from the

reference mean. Regions where differences are statistically significant in the VR-CESM dataset are identified with stippling.

Overall, VR-CESM accurately captures the spatial patterns of precipitation and its indices. As expected, the majority of precipitation is distributed along the northwest coast and the mountainous regions of the Cascades and the Sierra Nevada. Nonetheless, several apparent biases are present:

First, VR-CESM significantly overestimates Pr over dry regions with differences between 0.2 mm to 1.5 mm, and over the eastern flank of the Cascades and on both sides of the Sierra Nevada (with relative differences reaching 50%-150%). As with many regional models, VR-CESM is “dreary” and exhibits too many precipitation days ($R_{1mm}, Pr \geq 1 \text{ mm/day}$ and $R_{5mm}, 1 \text{ mm/day} \leq Pr \leq 5 \text{ mm/day}$) (see Figure 3) (Stephens et al. 2010). Nonetheless, over most regions the relative contribution of each precipitation frequency subset to total precipitation ($F_{1mm}, F_{5mm}, F_{10mm}, F_{20mm}$ and F_{40mm}) agrees well, suggesting that the frequency distribution describing precipitation intensity is accurately simulated almost everywhere.

Second, the spatial pattern of precipitation intensity (SDII) agrees well between VR-CESM and references with agreement everywhere except in the Great Plains (the eastern edge of our domain) and in California’s Central Valley. The Great Plains is not a focus of this study, but the suppressed intensity is primarily during the warm season (April-September) and so likely represents a failure of the convection scheme to adequately simulate variability in this region. This bias is also observed in 0.25° uniform-resolution CESM simulations (Small et al. 2014), and so is not a symptom of the eastern edge of the variable-resolution transition region.

However, the grossly exaggerated intensity over the western flank of the Sierra Nevada through California’s Central Valley does merit some additional discussion. Here, the overestimation of precipitation and enhanced intensity is associated with too many extreme precipitation events ($Pr > 20 \text{ mm/day}$) (see Figure 4, F_{40mm} and F_{xmm}). This bias is related to exaggerated orographic uplift

256 (upslope winds) and triggers a dry bias along the eastern flank of the Sierras. Similar biases in
257 simulating extreme precipitation over topographically complex regions have also been found in
258 high-resolution RCM simulations, and have been primarily attributed to excessively strong winds
259 (Walker and Diffenbaugh 2009; Singh et al. 2013). This issue may be further impacted by the
260 diagnostic treatment of precipitation in CAM5 (Morrison and Gettelman 2008; Gettelman et al.
261 2008).

262 The representation of precipitation in VR-CESM over California was also discussed in Huang
263 et al. (2016), where it was observed that VR-CESM simulations at 0.25° adequately represented
264 regional climatological patterns with high spatial correlation. VR-CESM demonstrated compa-
265 rable performance to WRF at 27 km (which was forced with ERA-Interim reanalysis), but still
266 overestimated overall winter precipitation compared to reference datasets (by about 25%-35%),
267 with the largest differences over the western edge of the Sierra Nevada. This bias is not allevi-
268 ated by simply increasing the spatial resolution, as experimental VR-CESM simulations at 14km,
269 7km and 3.5km show only modest improvement (Alan M. Rhoades, personal communication).
270 This suggests that the bias might be related with more complex dynamic processes rather than
271 treatment of the orographic effects.

272 CESM at 1° resolution was also assessed in order to better understand the impacts of resolution.
273 Overall, we find that precipitation patterns over complex topography are poorly represented in the
274 1° dataset and do not capture spatial patterns induced by orographic effects. Over the Cascades
275 and Sierra Nevada, total precipitation is grossly underestimated by the 1° data, even when com-
276 pared to coarsened VR-CESM, gridded and reanalysis datasets (see the supplement [Point to exact
277 figure]). Precipitation has otherwise been smoothed out over the coastal areas and the mountainous
278 regions of the northwest U.S when simulated with CESM at coarse resolution. This result clearly
279 underscores the benefits of high resolution (particularly the representation of topography) in sim-

280 ulating precipitation features. Results are also provided in the supplement for the output from
281 a globally-uniform CESM run at 0.25° spatial resolution with the finite volume (FV) dynamical
282 core (Wehner et al. 2014), which exhibits similar performance to VR-CESM (see the supplement
283 [[Point to exact figure](#)]). Overall, 0.25° resolution appears to provide the best tradeoff between
284 accuracy and computational cost, as coarser resolution does not correctly represent precipitation
285 features and higher resolution does not appear to substantially improve model accuracy (at least in
286 this version of CAM).

287 We have also assessed the impact of the ENSO signal within the historical VR-CESM runs by
288 differencing the precipitation fields between the warm phase (i.e. El Niño) and cool phase (i.e.
289 La Niña), compared to references (see the supplement [[point to exact figure](#)]). ENSO exhibits a
290 weaker signal for observational precipitation, compared to VR-CESM, which might suggest that
291 the model exaggerates ENSO's impact on precipitation, especially over the northwest U.S. The
292 improvement of ENSO in the model is directly proportional to the representation of ENSO-forced
293 precipitation anomalies (AchutaRao and Sperber 2006).

294 **5. Drivers of Climatological Precipitation Change**

295 The remainder of this paper now focuses on model predictions of change over the 21st cen-
296 tury. Precipitation has been observed and modeled to be modified in character at both global and
297 regional scales under climate change. The observed intensification of heavy precipitation events
298 over the recent past for the majority of Northern Hemisphere land areas is primarily attributed
299 to increases in GHGs (Min et al. 2011). GHGs drive radiative changes in the lower troposphere,
300 increase SSTs and lead to increased evaporation, all of which then impact the character of precip-
301 itation events (Allen and Ingram 2002; Sugi and Yoshimura 2004). Several studies have argued
302 that precipitation extremes will intensify continuously through the end of 21st century in both dry

303 and wet regions, although the extent of this change will be spatially heterogeneous (Donat et al.
304 2016).

305 In accordance with the Clausius-Clapeyron (C-C) relationship, saturation vapor pressure in the
306 atmosphere is expected to increase by $\sim 7\%$ for each 1°C increase in temperature (Allan and So-
307 den 2008). As long as a source of water vapor is present, a corresponding increase in atmospheric
308 water vapor content is expected. Naturally, evaporation over the ocean will increase with climate
309 warming, but increases in water vapor content over land may be constrained by soil moisture
310 (Cayan et al. 2010). When specific humidity is high, heavy rain events become more probable,
311 even if total precipitation is decreasing (Trenberth 2011). This suggests that global total precipita-
312 tion is expected to increase at a slower rate than precipitation extremes (Allan and Soden 2008). In
313 accordance with previous studies (e.g. Allan and Soden (2008); O’Gorman and Schneider (2009);
314 Min et al. (2011)), changes to extreme precipitation follow the C-C relationship more closely than
315 total precipitation amount (Trenberth et al. 2003). However, there is still substantial uncertainty
316 regarding the magnitude of this change, since precipitation extremes are also dependent on factors
317 such as the vertical velocity profile and temperature (O’Gorman and Schneider 2009).

318 With overland water vapor constrained by soil moisture content, changes to moderate or heavy
319 precipitation events over the WUS are mainly the result of increased large-scale vapor transport
320 from the eastern Pacific Ocean rather than directly from evaporation, typically associated with
321 atmospheric rivers (ARs) and/or orographic uplift (Trenberth et al. 2003; Neiman et al. 2008).
322 Warming may lead to enhancement of the storm track, which would increase ARs along the U.S.
323 west coast with increased air water vapor content in the future (Dettinger 2011; Gao et al. 2015).

324 The precipitation of the WUS has strong inter-annual variability caused by large-scale atmo-
325 spheric circulation mainly associated with the ENSO (Leung et al. 2003b). As a significant
326 driver of precipitation, ENSO modulates the storm track behavior over western U.S. with a north-

327 west/southwest precipitation dipole (Gershunov and Barnett 1998), as discussed in 6d. The pro-
328 jected SSTs used in this study emerge from one possible realization of ENSO. However, there is
329 still substantial uncertainty regarding how El Niño will change under global warming (Fedorov
330 and Philander 2000; Guilyardi et al. 2009), which is a source of uncertainty in our results. Capo-
331 tondi (2013) showed that the diversity of El Niño characteristics in CCSM4 is comparable to what
332 was found in observations, although, as found by Deser et al. (2012c), the overall magnitude of
333 ENSO in CCSM4 is overestimated by 30% over the preindustrial time period.

334 6. Results

335 a. Mean climatology

336 Differences in the mean climate of the WUS, as predicted by VR-CESM across time periods,
337 are depicted in Figure 5. Since the character of WUS precipitation has a strong seasonal contrast,
338 changes to mean precipitation, near-surface temperature and near-surface relative humidity are
339 depicted for what we refer to as the cool season (October to March) and the warm season (April
340 to September).

341 As a result of enhanced GHG concentrations, mean annual near-surface temperature (T_{avg})
342 increases by between 1.5 to 3.5K from hist to mid and between 4 to 7.5K from hist to end.
343 Despite the large spatial variation in mean seasonal temperatures, the observed differences in
344 mean temperature across time periods are fairly uniform, particularly over the ocean and in coastal
345 regions. Away from the coast there is a weak gradient in the temperature change field, with the
346 largest increase in temperatures occurring towards the northeast during the cool season and towards
347 the north during the warm season. The increase in temperature is also about 0.5K and 1.0K larger
348 during the warm season compared to the cool season for mid and end, respectively.

349 Overall, future RH is constrained closely to hist since it is governed by competing increases
350 in temperature and atmospheric water vapor content. Although RH increases monotonically over
351 the ocean in response to increased evaporation, over land the character is more heterogeneous: In
352 general, RH tends to increase in regions where Tavg increase is constrained below ~ 2 K, but de-
353 crease when Tavg anomaly exceeds ~ 2 K. The decrease in these regions is on the order of 2% and
354 3-6%, for mid and end respectively. In fact, trends in RH are spatially consistent with tempera-
355 ture increase but opposite in magnitude with a spatial correlation coefficient of approximately 0.8.
356 This suggests that continental evaporation and oceanic water vapor transport are insufficient vapor
357 sources when temperature reaches a certain level, consistent with the observation of Joshi et al.
358 (2008). This effect has also been observed in results by Rowell and Jones (2006) over continental
359 and southeastern Europe and Simmons et al. (2010) over low-latitude and midlatitude land areas.

360 In response to these changes to temperature and RH, from hist to mid mean precipitation over
361 the entire domain exhibited a 0.2-0.6 mm/day increase during the cool season. The largest changes
362 were over northwest, where cool-season precipitation emerges from large-scale patterns (namely,
363 atmospheric rivers and associated storm systems)(Trenberth et al. 2003; Neiman et al. 2008). Over
364 the warm season, where precipitation in the WUS is primarily from convection, the increase was
365 around 0.2 mm/day through the intermountain west and southwest with drying through the north-
366 west (a decrease in mean precipitation of 0.2 mm/day). These trends largely hold and intensify
367 through end, except in the intermountain west and southwest regions where precipitation again
368 falls to historical levels. Statistical significance of these results is depicted in Figure 6.

369 The increase in cool season precipitation in the northwest is largely driven by increased inte-
370 grated vapor transport (IVT) (see Figure 8a,b) during extreme precipitation events. As observed
371 in previous studies, IVT is particularly useful for understanding extreme precipitation events that
372 arise from large-scale meteorological features (Ralph et al. 2004; Leung and Qian 2009; Dettinger

373 2011). IVT is composed of humidity and wind velocity, which are both impacted by the climate
374 change signal, as plotted in Figure 8b. Over the eastern Pacific, we observe increases in both water
375 vapor content and wind speed, which are in turn responsible for increases to IVT in the Pacific
376 Northwest. However, over the continent we see a weakening of the westerlies overland driven
377 by a reduced meridional temperature contrast. The increased cool-season IVT does not manifest
378 strongly along the Pacific coast off of California, where IVT is much smaller on average and is
379 primarily modulated by ENSO.

380 Changes in precipitation over the intermountain west and southwest during the warm season are
381 primarily associated with convective processes and so are directly impacted by variations in RH.
382 As shown in Figure 5, RH increases through mid-century in this region (although with modest
383 significance) and then significantly decreases through end-of-century over most the study area
384 (except over where soil moisture was already low in hist). This results in a modest increase in
385 precipitation through mid-century followed by a return to historical precipitation amounts by end-
386 of-century. Further climate warming is expected to further decrease RH and drive increased aridity
387 in this region.

388 *b. Precipitation indices*

389 We now analyze observed changes to the precipitation indices given in Table 1. For each index,
390 the change for each period, yearly averaged over all ensemble members are plotted in Figure 6 (for
391 the indices that quantify precipitation days) and Figure 7 (for the indices describing precipitation
392 amounts).

393 On comparing hist and mid, it is clear that the number of rainy days and frequency of non-
394 extreme precipitation events (≤ 10 mm/day) have increased significantly (about 10-15%) over the
395 southwest and intermountain west, which is less obvious between mid and end. On the contrary,

396 the frequency of non-extreme precipitation has decreased significantly over the northwest region
397 and the eastern areas of the Montana, Wyoming and Oregon (by about 10%). The increase in
398 the frequency of these non-extreme precipitation events explain the observed change to mean
399 precipitation exhibited in Figure 5, and are largely associated with warm season mesoscale storm
400 systems.

401 Although essentially all regions exhibit an increase in the extreme precipitation events ($\text{Pr} \geq 10$
402 mm/day), this increase is only statistically significant through the intermountain west and in the
403 Pacific northwest (for $\text{Pr} \geq 20$ mm/day). When comparing mid to end, there is a clear and sig-
404 nificant increase in extreme precipitation events over the northwest coast ($\sim 20\text{-}30\%$) and eastern
405 flank of the Cascades ($> 40\%$). This result is consistent with the result of Dominguez et al. (2012),
406 who observe a robust increase in winter precipitation extremes toward the latter half of the 21st
407 century with an ensemble of RCMs. The increase in the northwest is accompanied by a decrease
408 in non-extreme precipitation days, indicative of drying over the warm season.

409 Notably, our results show no significant changes in mean precipitation or precipitation extremes
410 are predicted for California. In fact, the precipitation signal under a warmer climate is more
411 ambiguous for California (Neelin et al. 2013) in light of the extreme variability of the region on
412 interannual time scales (Dettinger 2011). Kim (2005) found that under global warming, heavy
413 precipitation events increase in frequency in the mountainous regions of the northern California
414 Coastal Range and the Sierra Nevada. However, our results show a small decrease in extreme
415 precipitation over the Sierra Nevada (although the decrease is not statistically significant). This
416 leads us to the likely conclusion (particularly in light of VR-CESM's own biases in this region)
417 that projections in this region are highly dependent on model formulation.

418 For the most extreme precipitation events ($\text{Pr} \geq 40$ mm/day), there is a statistically significant
419 increase along the northwest coast ($\geq 60\%$), the Cascades ($\sim 50\%$) and Northern Rockies ($\geq 60\%$)

420 by end-of-century. Significant increases are also apparent along the Klamath range in California
421 of about 20-40% from hist to end. Changes in accumulated precipitation for these events are con-
422 sistent with the change in their frequency (see Figure 7). With a projected increase of temperatures
423 in this region of 4-5 K over the cool season, this increase is in excess of the 7% per degree change
424 that would be anticipated from the C-C relationship (Figure 8a). In this case, the probable cause
425 of this excess is due to the intensification of the storm track along the coast discussed in section
426 6a.

427 *c. Regional precipitation frequency distributions*

428 To further investigate the regional heterogeneity of changing precipitation, frequency distribu-
429 tions of daily rainfall for rainy days are plotted in Figure 9 for (a) the Pacific northwest, including
430 Washington and Oregon, (b) central and southern California, (c) the intermountain west, including
431 Nevada and Utah and (d) the southwest, including Arizona and New Mexico. Frequency plots
432 are developed using simulation outputs at all grid points within each region. Results here mirror
433 our earlier discussion. Over the northwest, precipitation intensity increases with a shift towards
434 greater frequency of the most extreme precipitation days, especially by end-of-century, accompa-
435 nied by a reduction in non-extreme precipitation days. No significant shifts can be observed for
436 the California region. Over the intermountain west, there is a similar trend towards more extreme
437 precipitation as in the northwest, but with no reduction in warm season non-extreme precipitation
438 days. Finally, in the southwest, precipitation is more frequent, but the response is weaker than that
439 observed in the intermountain west.

440 *d. Disentangling the direct climate signal from ENSO and PDO*

441 As discussed earlier, this study assumes a fixed pattern of SSTs that is consistent across all
442 ensemble members and incorporates certain assumptions on the character of ENSO through the
443 end-of-century that arise from the coupled model. The phase of ENSO is well known to have
444 important repercussions for precipitation extremes (Larkin and Harrison 2005; Allan and Soden
445 2008; Maloney et al. 2014; Yoon et al. 2015). In particular, Cai et al. (2014) found a significant
446 increase in extraordinary precipitation events through the eastern Pacific Ocean in the 21st century
447 within the CMIP5 ensemble, associated with increasing frequency of extreme El Niño events due
448 to greenhouse warming. To better understand how ENSO has impacted our results, we now turn
449 our attention to understanding how precipitation extremes behave in response to the phase of
450 ENSO.

451 In our study, mean SSTs over the Niño 3.4 region are 26.83, 28.62 and 30.54°C for hist, mid and
452 end respectively. Based on the ONI index values, the mean SST anomalies over Niño 3.4 region
453 are 1.38, 1.71 and 2.30 K during El Niño years, and -1.16, -1.62 and -1.43 K during La Niña years,
454 again for hist, mid and end. It is apparent within that within this dataset the magnitude of SST
455 anomalies associated with ENSO has intensified. SST anomalies of each year and each month,
456 and their associated spatial pattern when averaged over the warm and cool phases of ENSO can
457 be found in the supplement, suggesting an increasing frequency of El Niño through mid and an
458 almost doubled frequency of La Niña during mid and end compared to the hist.

459 [Huang: As SSTs increase in the future, is not it normal for the anomaly of ENSO to be increased
460 to compensate the changes of water vapor capacity? Might email Neale about this]

461 Differences in mean precipitation and associated indices taken between the warm phase (i.e.
462 El Niño) and cool phase (i.e. La Niña) of ENSO are provided in Figure 10 for the cool seasons

from hist, mid and end. During the El Niño phase, intensified mean precipitation is expected over California and the southwest (Hamlet and Lettenmaier 2007), accompanied by reduced precipitation intensity over the northwest. In the La Niña phase, this pattern is reversed, with wetter conditions in the northwest and a drier southwest. Consequently, ENSO is associated with a northwest/southwest precipitation dipole, triggered by ENSO's modification of the storm track (Gershunov and Barnett 1998; Leung et al. 2003b), along with modulation of the enhanced precipitation variability (Cayan et al. 1999; Kahya and Dracup 1994). Strengthening storm patterns associated with ENSO are also found by Maloney et al. (2014) over California using CMIP5 output under RCP8.5. This dipole is also apparent in the frequency of rainy days and extreme precipitation events.

The impact of ENSO can also be seen in the IVT difference that arises between El Niño and La Niña phases in each time period (see Figure 11) and the accompanying 850 hPa wind patterns. During the El Niño phase, there is an increase in on-shore moisture flux over California that triggers a returning circulation through the northwest. This suggests that understanding moisture flux regulation from ENSO is a very important contributor to the character of future precipitation extremes.

Based on the above results, it is apparent that the magnitude of the effects of ENSO is comparable or even higher than the impacts of climate forcing – that is, shifts in the future character of ENSO would have more dire implications for precipitation extremes than shifts in mean climatological forcing. To investigate this further, linear regression has applied at each grid point using a simple linear model that incorporates the phase of ENSO (using the Niño 3.4 SST anomaly) and the underlying climate forcing (from mean GHG concentration). The precipitation indices are used as response variables. The significance of these two factors was then obtained from ANOVA (analysis of variance) output (see the supplement [Paul: Point to lm_fit_pvalue]). The magnitude

487 of the response associated with each factor was also computed (see the supplement [Paul: Point
488 to [wd_lmfit_coef_enso_ghg](#)]). As expected, the ENSO forcing matches most closely with the dif-
489 ference between El Niño and La Niña (see Figure 11). Hence, we observe that ENSO is a major
490 driver of precipitation character through California, the intermountain west and the southwest and
491 does have an impact on mean precipitation through the Cascades. In contrast, the impacts of cli-
492 mate forcing are visually similar to the pattern of the difference between the different time periods
493 (see Figure 6), and primarily impacts both extreme and non-extreme precipitation in the northwest
494 and intermountain west.

495 We have also assessed the impacts of the Pacific Decadal Oscillation (PDO) on precipitation
496 and observed only a weak correlation between the PDO pattern and precipitation. That is, pre-
497 cipitation features did not change substantially between the cool phase or warm phase of PDO
498 when examining hist data. However, when in phase with ENSO, PDO did have a notable impact
499 over the northwest. This coupled effect has been found by studies such as Gershunov and Barnett
500 (1998), who observed that ENSO and PDO can “reinforce” each other, with PDO responding to
501 the same internal atmospheric variability as ENSO (Pierce 2002). In our simulations, there were
502 roughly an equal number of positive PDO years and negative PDO years in the data from each
503 time period, but since SSTs were fixed among ensemble members, the 26 year simulation period
504 might be insufficient to account for the variability of PDO. Therefore, in this study we draw no
505 conclusions on the impact of PDO.

506 7. Discussion and Summary

507 In this study, an ensemble of 26-year simulations have been conducted using VR-CESM with
508 finest local grid resolution of $\sim 0.25^\circ$ to assess the changing character of precipitation over the

509 21st Century in the WUS. Climate forcing for future projections is prescribed under the RCP8.5
510 “business-as-usual” scenario.

511 Evaluated against historical reanalysis and gridded data, VR-CESM was found to accurately cap-
512 ture the spatial patterns of precipitation, including precipitation frequency and intensity, although it
513 exhibited an overestimation of precipitation over the eastern flank of the Cascades, throughout Cal-
514 ifornia’s Central Valley and along the Sierra Nevada. Nonetheless, there was clear improvement in
515 the representation of precipitation features when compared with coarse 1° resolution simulations.

516 Both mean changes to precipitation and distributions of both non-extreme and extreme events,
517 projected by the VR-CESM model under climate forcing, have been investigated. Although con-
518 strained by water influx and soil moisture, changes to extreme precipitation are hypothesized to
519 follow the C-C relationship more closely than total precipitation amount.

520 From the VR-CESM results, the warming response to the RCP8.5 climate forcing exhibited
521 roughly uniform character, although warming was more pronounced away from the coast and to
522 the north. Future relative humidity (RH) was observed to be constrained by competing increases
523 in both temperature and atmospheric water vapor content. RH tended to increase in regions where
524 average temperature increase was below ~2 K, and decrease when average temperature increase
525 exceeded ~2 K. This suggests that continental evaporation and oceanic water vapor transport
526 are insufficient vapor sources to maintain RH levels above a certain threshold temperature. In
527 response, mean precipitation increase is fairly inhomogeneous, with a more pronounced increase
528 in the Northwest where vapor transport is enhanced.

529 Over the intermountain west and southwest, an increase in warm season RH through mid-century
530 led to a statistically significant increase in precipitation and non-extreme rainy days due to in-
531 creased convection. This increase levels off through end-of-century, when increased temperatures
532 are observed to drive a reduction in RH. Nonetheless, there is a significant increase in extreme

533 precipitation episodes (≥ 10 mm/day) over the intermountain west which is not observed in the
534 southwest.

535 Over the northwest, there is a clear shift from non-extreme precipitation events to extreme pre-
536 cipitation events associated with a moistening of the cool season and drying through the warm
537 season. Although the total number of annual precipitation days remains relatively constant, there
538 is a decrease in < 10 mm/day precipitation days and an increase in > 20 mm/day precipitation
539 days. In each case, the change is on the order of 10 days/year. This change is driven by increased
540 IVT over the eastern Pacific, associated with atmospheric river (AR) episodes. Increased drying
541 over the warm season is driven by a reduction in RH. Increased cool season precipitation extremes
542 in this region tend to result in high runoff events, which are in turn associated with a greater chance
543 of flooding, particularly from rain-on-snow events.

544 Over California, except along the northernmost coast, there is no clear climate signal apparent
545 in the mean precipitation or extremes. Interannual variability in this region associated with ENSO
546 dominates precipitation patterns throughout the historical period and the 21st century. ENSO
547 drives precipitation behavior by modulating the midlatitudinal storm track in this region. In par-
548 ticular, during the El Niño phase, there is an increase in on-shore moisture flux over California
549 that triggers a returning circulation through the northwest. The results over California highlight
550 the importance of understanding the response of ENSO to climate change (which is still largely
551 inconsistent in CMIP5 climate models and so is a key source of uncertainty in our results), since
552 variations in the magnitude or structure of ENSO will have immediate consequences for precipi-
553 tation in this region.

554 The projected SSTs utilized for this study through end-of-century suggest that SST anomalies
555 associated with ENSO will intensify. The impacts of ENSO are wide-reaching, with a statis-
556 tically significant response observed in the character of precipitation throughout California, the

557 intermountain west and the southwest regions, as well as impacting mean precipitation through
558 the Cascades. In contrast, the significance of climate forcing (when compensating for ENSO)
559 largely matched the differences observed between time periods, and had its greatest impact on
560 both extreme and non-extreme precipitation in the northwest and intermountain west.

561 *Acknowledgments.* The authors would like to thank Michael Wehner for sharing the 0.25°
562 uniform-resolution CESM dataset, and his many suggestions. The authors also want to thank Alan
563 M. Rhoades for providing the simulation output and providing his feedback on the manuscript.
564 We acknowledge the substantial efforts behind the datasets used in this study, including UW,
565 NCDC and NARR. The simulation data used is available by request at xyhuang@ucdavis.edu.
566 This project is supported in part by the University of California, Davis and by the Department of
567 Energy “Multiscale Methods for Accurate, Efficient, and Scale-Aware Models of the Earth Sys-
568 tem” project. Support also comes from the California Agricultural Experiment Station (project
569 CA-D-LAW-2203-H).

570 References

- 571 AchutaRao, K., and K. R. Sperber, 2006: ENSO simulation in coupled ocean-atmosphere
572 models: are the current models better? *Climate Dynamics*, **27** (1), 1–15, doi:10.1007/
573 s00382-006-0119-7.
- 574 Allan, R. P., and B. J. Soden, 2008: Atmospheric warming and the amplification of precipitation
575 extremes. *Science*, **321** (5895), 1481–1484, doi:10.1126/science.1160787.
- 576 Allen, M. R., and W. J. Ingram, 2002: Constraints on future changes in climate and the hydrologic
577 cycle. *Nature*, **419** (6903), 224–232, doi:10.1038/nature01092.

- 578 Ashfaq, M., D. Rastogi, R. Mei, S.-C. Kao, S. Gangrade, B. Naz, and D. Touma, 2016: High-
579 resolution ensemble projections of near-term regional climate over the continental united states.
580 *Journal of Geophysical Research: Atmospheres*, doi:10.1002/2016JD025285.
- 581 Bell, J. L., L. C. Sloan, and M. A. Snyder, 2004: Regional changes in extreme climatic events:
582 a future climate scenario. *Journal of Climate*, **17** (1), 81–87, doi:10.1175/1520-0442(2004)
583 017⟨0081:RCIECE⟩2.0.CO;2.
- 584 Cai, W., and Coauthors, 2014: Increasing frequency of extreme El Niño events due to greenhouse
585 warming. *Nature Climate Change*, **4** (2), 111–116, doi:10.1038/nclimate2100.
- 586 Caldwell, P., 2010: California wintertime precipitation bias in regional and global climate
587 models. *Journal of Applied Meteorology and Climatology*, **49** (10), 2147–2158, doi:10.1175/
588 2010JAMC2388.1.
- 589 Capotondi, A., 2013: ENSO diversity in the NCAR CCSM4 climate model. *Journal of Geophysi-
590 cal Research: Oceans*, **118** (10), 4755–4770, doi:10.1002/jgrc.20335.
- 591 Cayan, D. R., T. Das, D. W. Pierce, T. P. Barnett, M. Tyree, and A. Gershunov, 2010: Future
592 dryness in the southwest US and the hydrology of the early 21st century drought. *Proceedings
593 of the National Academy of Sciences*, **107** (50), 21 271–21 276, doi:10.1073/pnas.0912391107.
- 594 Cayan, D. R., K. T. Redmond, and L. G. Riddle, 1999: ENSO and hydrologic extremes in the
595 western United States. *Journal of Climate*, **12** (9), 2881–2893, doi:10.1175/1520-0442(1999)
596 012⟨2881:EAHEIT⟩2.0.CO;2.
- 597 Collins, M., and Coauthors, 2010: The impact of global warming on the tropical Pacific Ocean
598 and El Niño. *Nature Geoscience*, **3** (6), 391–397, doi:10.1038/ngeo868.

- 599 Dennis, J., and Coauthors, 2011: CAM-SE: A scalable spectral element dynamical core for the
600 Community Atmosphere Model. *International Journal of High Performance Computing Applications*,
601 1094342011428142, doi:10.1177/1094342011428142.
- 602 Deser, C., R. Knutti, S. Solomon, and A. S. Phillips, 2012a: Communication of the role of natural
603 variability in future North American climate. *Nature Climate Change*, **2** (11), 775–779, doi:
604 10.1038/nclimate1562.
- 605 Deser, C., A. Phillips, V. Bourdette, and H. Teng, 2012b: Uncertainty in climate change pro-
606 jections: the role of internal variability. *Climate Dynamics*, **38** (3-4), 527–546, doi:10.1007/
607 s00382-010-0977-x.
- 608 Deser, C., and Coauthors, 2012c: ENSO and Pacific decadal variability in the Community
609 Climate System Model version 4. *Journal of Climate*, **25** (8), 2622–2651, doi:10.1175/
610 JCLI-D-11-00301.1.
- 611 Dettinger, M., 2011: Climate change, atmospheric rivers, and floods in California—a mul-
612 timodel analysis of storm frequency and magnitude changes. Wiley Online Library, doi:
613 10.1111/j.1752-1688.2011.00546.x.
- 614 Diffenbaugh, N. S., J. S. Pal, R. J. Trapp, and F. Giorgi, 2005: Fine-scale processes regulate the re-
615 sponse of extreme events to global climate change. *Proceedings of the National Academy of Sci-
616 ences of the United States of America*, **102** (44), 15 774–15 778, doi:10.1073/pnas.0506042102.
- 617 DiNezio, P. N., B. P. Kirtman, A. C. Clement, S.-K. Lee, G. A. Vecchi, and A. Wittenberg, 2012:
618 Mean climate controls on the simulated response of ENSO to increasing greenhouse gases.
619 *Journal of Climate*, **25** (21), 7399–7420, doi:10.1175/JCLI-D-11-00494.1.

- 620 Dominguez, F., E. Rivera, D. Lettenmaier, and C. Castro, 2012: Changes in winter precipitation
621 extremes for the western United States under a warmer climate as simulated by regional climate
622 models. *Geophysical Research Letters*, **39** (5), doi:10.1029/2011GL050762.
- 623 Donat, M. G., A. L. Lowry, L. V. Alexander, P. A. OGorman, and N. Maher, 2016: More ex-
624 treme precipitation in the world's dry and wet regions. *Nature Climate Change*, doi:10.1038/
625 nclimate2941.
- 626 Duffy, P., and Coauthors, 2006: Simulations of present and future climates in the western United
627 States with four nested regional climate models. *Journal of Climate*, **19** (6), 873–895, doi:
628 10.1175/JCLI3669.1.
- 629 Duli re, V., Y. Zhang, and E. P. Salath  Jr, 2011: Extreme precipitation and temperature over
630 the US Pacific Northwest: A comparison between observations, reanalysis data, and regional
631 models. *Journal of Climate*, **24** (7), 1950–1964, doi:10.1175/2010JCLI3224.1.
- 632 Easterling, D. R., G. A. Meehl, C. Parmesan, S. A. Changnon, T. R. Karl, and L. O. Mearns, 2000:
633 Climate extremes: observations, modeling, and impacts. *science*, **289** (5487), 2068–2074, doi:
634 10.1126/science.289.5487.2068.
- 635 Fedorov, A. V., and S. G. Philander, 2000: Is El Ni o changing? *Science*, **288** (5473), 1997–2002.
- 636 Fox-Rabinovitz, M., J. C te, B. Dugas, M. D qu , and J. L. McGregor, 2006: Variable resolution
637 general circulation models: Stretched-grid model intercomparison project (SGMIP). *Journal of*
638 *Geophysical Research: Atmospheres (1984–2012)*, **111** (D16), doi:10.1029/2005JD006520.
- 639 Fox-Rabinovitz, M. S., G. L. Stenchikov, M. J. Suarez, and L. L. Takacs, 1997: A finite-
640 difference GCM dynamical core with a variable-resolution stretched grid. *Monthly Weather
641 Review*, **125** (11), 2943–2968, doi:10.1175/1520-0493(1997)125<2943:AFDGDC>2.0.CO;2.

- 642 Frei, C., R. Schöll, S. Fukutome, J. Schmidli, and P. L. Vidale, 2006: Future change of precipitation extremes in Europe: Intercomparison of scenarios from regional climate models. *Journal*
643
644 *of Geophysical Research: Atmospheres (1984–2012)*, **111** (D6), doi:10.1029/2005JD005965.
- 645 Gao, Y., J. Lu, L. R. Leung, Q. Yang, S. Hagos, and Y. Qian, 2015: Dynamical and thermodynamic
646 modulations on future changes of landfalling atmospheric rivers over western North America. *Geophysical Research Letters*, **42** (17), 7179–7186, doi:10.1002/2015GL065435.
- 647
648 Gates, W. L., 1992: AMIP: The Atmospheric Model Intercomparison Project. *Bulletin of the American Meteorological Society*, **73**, 1962–1970.
- 649
650 Gershunov, A., and T. P. Barnett, 1998: Interdecadal modulation of ENSO teleconnections. *Bulletin of the American Meteorological Society*, **79** (12), 2715–2725, doi:10.1175/1520-0477(1998)079<2715:IMOET>2.0.CO;2.
- 651
652
653 Gettelman, A., H. Morrison, and S. J. Ghan, 2008: A new two-moment bulk stratiform cloud microphysics scheme in the Community Atmosphere Model, version 3 (CAM3). Part II: Single-column and global results. *Journal of Climate*, **21** (15), 3660–3679, doi:10.1175/2008JCLI2116.1.
- 654
655
656 Grodsky, S. A., J. A. Carton, S. Nigam, and Y. M. Okumura, 2012: Tropical Atlantic biases in CCSM4. *Journal of Climate*, **25** (11), 3684–3701, doi:10.1175/JCLI-D-11-00315.1.
- 657
658
659 Guilyardi, E., A. Wittenberg, A. Fedorov, M. Collins, C. Wang, A. Capotondi, G. J. Van Oldenborgh, and T. Stockdale, 2009: Understanding El Niño in ocean-atmosphere general circulation models. *Bulletin of the American Meteorological Society*, **90** (3), 325, doi:10.1175/2008BAMS2387.1.

- 663 Hamlet, A. F., and D. P. Lettenmaier, 2005: Production of temporally consistent gridded precip-
664 itation and temperature fields for the continental United States. *Journal of Hydrometeorology*,
665 **6** (3), 330–336, doi:10.1175/JHM420.1.
- 666 Hamlet, A. F., and D. P. Lettenmaier, 2007: Effects of 20th century warming and climate
667 variability on flood risk in the western US. *Water Resources Research*, **43** (6), doi:10.1029/
668 2006WR005099.
- 669 Hegerl, G. C., F. W. Zwiers, P. A. Stott, and V. V. Kharin, 2004: Detectability of anthropogenic
670 changes in annual temperature and precipitation extremes. *Journal of Climate*, **17** (19), 3683–
671 3700, doi:10.1175/1520-0442(2004)017<3683:DOACIA>2.0.CO;2.
- 672 Huang, X., A. M. Rhoades, P. A. Ullrich, and C. M. Zarzycki, 2016: An evaluation of the variable
673 resolution-CESM for modeling California’s climate. *Journal of Advances in Modeling Earth
674 Systems*, doi:10.1002/2015MS000559.
- 675 Huang, X., and P. A. Ullrich, 2016: Irrigation impacts on California’s climate with the
676 variable-resolution CESM. *Journal of Advances in Modeling Earth Systems*, doi:10.1002/
677 2016MS000656.
- 678 Hurrell, J. W., J. J. Hack, D. Shea, J. M. Caron, and J. Rosinski, 2008: A new sea surface temper-
679 ature and sea ice boundary dataset for the Community Atmosphere Model. *Journal of Climate*,
680 **21** (19), 5145–5153.
- 681 Hurrell, J. W., and Coauthors, 2013: The community earth system model: A framework for col-
682 laborative research. *Bulletin of the American Meteorological Society*, **94** (9), 1339–1360, doi:
683 10.1175/BAMS-D-12-00121.1.

- 684 Jha, B., Z.-Z. Hu, and A. Kumar, 2014: SST and ENSO variability and change simulated in
685 historical experiments of CMIP5 models. *Climate Dynamics*, **42** (7-8), 2113–2124, doi:10.1007/
686 s00382-013-1803-z.
- 687 Joseph, R., and S. Nigam, 2006: ENSO evolution and teleconnections in IPCC's twentieth-century
688 climate simulations: Realistic representation? *Journal of Climate*, **19** (17), 4360–4377, doi:
689 10.1175/JCLI3846.1.
- 690 Joshi, M. M., J. M. Gregory, M. J. Webb, D. M. Sexton, and T. C. Johns, 2008: Mechanisms for
691 the land/sea warming contrast exhibited by simulations of climate change. *Climate Dynamics*,
692 **30** (5), 455–465, doi:10.1007/s00382-007-0306-1.
- 693 Kahya, E., and J. A. Dracup, 1994: The influences of type 1 El Nino and La Nina events on
694 streamflows in the Pacific southwest of the United States. *Journal of Climate*, **7** (6), 965–976,
695 doi:10.1175/1520-0442(1994)007<0965:TIOTEN>2.0.CO;2.
- 696 Kao, H.-Y., and J.-Y. Yu, 2009: Contrasting eastern-Pacific and central-Pacific types of ENSO.
697 *Journal of Climate*, **22** (3), 615–632.
- 698 Karl, T. R., N. Nicholls, and A. Ghazi, 1999: Clivar/GCOS/WMO workshop on indices and indi-
699 cators for climate extremes workshop summary. *Weather and Climate Extremes*, Springer, 3–7,
700 doi:10.1023/A:1005491526870.
- 701 Kharin, V. V., F. W. Zwiers, X. Zhang, and G. C. Hegerl, 2007: Changes in temperature and
702 precipitation extremes in the IPCC ensemble of global coupled model simulations. *Journal of*
703 *Climate*, **20** (8), 1419–1444, doi:10.1175/JCLI4066.1.

- 704 Kim, J., 2005: A projection of the effects of the climate change induced by increased CO₂ on
705 extreme hydrologic events in the western US. *Climatic Change*, **68** (1-2), 153–168, doi:10.
706 1007/s10584-005-4787-9.
- 707 Laprise, R., and Coauthors, 2008: Challenging some tenets of regional climate modelling. *Meteo-*
708 *rology and Atmospheric Physics*, **100** (1-4), 3–22, doi:10.1007/s00703-008-0292-9.
- 709 Larkin, N. K., and D. Harrison, 2005: On the definition of El Niño and associated seasonal average
710 US weather anomalies. *Geophysical Research Letters*, **32** (13), doi:10.1029/2005GL022738.
- 711 Latif, M., and N. S. Keenlyside, 2009: El Niño/Southern Oscillation response to global warming.
712 *Proceedings of the National Academy of Sciences*, **106** (49), 20 578–20 583, doi:10.1073/pnas.
713 0710860105.
- 714 Leung, L. R., L. O. Mearns, F. Giorgi, and R. L. Wilby, 2003a: Regional climate research: needs
715 and opportunities. *Bulletin of the American Meteorological Society*, **84** (1), 89–95, doi:10.1175/
716 BAMS-84-1-89.
- 717 Leung, L. R., and Y. Qian, 2009: Atmospheric rivers induced heavy precipitation and flooding in
718 the western US simulated by the WRF regional climate model. *Geophysical Research Letters*,
719 **36** (3), doi:10.1029/2008GL036445.
- 720 Leung, L. R., Y. Qian, and X. Bian, 2003b: Hydroclimate of the western United States based on
721 observations and regional climate simulation of 1981-2000. Part I: Seasonal statistics. *Journal*
722 *of Climate*, **16** (12), 1892–1911, doi:10.1175/1520-0442(2003)016<1892:HOTWUS>2.0.CO;2.
- 723 Maloney, E. D., and Coauthors, 2014: North American climate in CMIP5 experiments: part iii:
724 assessment of twenty-first-century projections. *Journal of Climate*, **27** (6), 2230–2270, doi:
725 10.1175/JCLI-D-13-00273.1.

- 726 Maurer, E., A. Wood, J. Adam, D. Lettenmaier, and B. Nijssen, 2002: A long-term hydrologically
727 based dataset of land surface fluxes and states for the conterminous United States. *Journal of*
728 *Climate*, **15 (22)**, 3237–3251, doi:10.1175/1520-0442(2002)015<3237:ALTHBD>2.0.CO;2.
- 729 McDonald, A., 2003: Transparent boundary conditions for the shallow-water equations: test-
730 ing in a nested environment. *Monthly Weather Review*, **131 (4)**, 698–705, doi:10.1175/
731 1520-0493(2003)131<0698:TBCFTS>2.0.CO;2.
- 732 Meehl, G. A., H. Teng, and G. Branstator, 2006: Future changes of El Niño in two global coupled
733 climate models. *Climate Dynamics*, **26 (6)**, 549–566, doi:10.1007/s00382-005-0098-0.
- 734 Mesinger, F., and K. Veljovic, 2013: Limited area NWP and regional climate modeling: a test
735 of the relaxation vs Eta lateral boundary conditions. *Meteorology and Atmospheric Physics*,
736 **119 (1-2)**, 1–16, doi:10.1007/s00703-012-0217-5.
- 737 Mesinger, F., and Coauthors, 2006: North American regional reanalysis. *Bulletin of the American*
738 *Meteorological Society*, **87**, 343–360.
- 739 Min, S.-K., X. Zhang, F. W. Zwiers, and G. C. Hegerl, 2011: Human contribution to more-intense
740 precipitation extremes. *Nature*, **470 (7334)**, 378–381, doi:10.1038/nature09763.
- 741 Morrison, H., and A. Gettelman, 2008: A new two-moment bulk stratiform cloud microphysics
742 scheme in the Community Atmosphere Model, version 3 (CAM3). Part I: Description and nu-
743 matical tests. *Journal of Climate*, **21 (15)**, 3642–3659, doi:10.1175/2008JCLI2105.1.
- 744 Neale, R. B., and Coauthors, 2010a: Description of the NCAR community atmosphere model
745 (CAM 5.0). *NCAR Tech. Note NCAR/TN-486+STR*.

- 746 Neale, R. B., and Coauthors, 2010b: Description of the NCAR Community Atmosphere Model
747 (CAM 5.0). NCAR Technical Note NCAR/TN-486+STR, National Center for Atmospheric Re-
748 search, Boulder, Colorado, 268 pp.
- 749 Neelin, J. D., B. Langenbrunner, J. E. Meyerson, A. Hall, and N. Berg, 2013: California winter
750 precipitation change under global warming in the Coupled Model Intercomparison Project phase
751 5 ensemble. *Journal of Climate*, **26** (17), 6238–6256, doi:10.1175/JCLI-D-12-00514.1.
- 752 Neiman, P. J., F. M. Ralph, G. A. Wick, J. D. Lundquist, and M. D. Dettinger, 2008: Meteorological
753 characteristics and overland precipitation impacts of atmospheric rivers affecting the
754 West Coast of North America based on eight years of SSM/I satellite observations. *Journal of
755 Hydrometeorology*, **9** (1), 22–47, doi:10.1175/2007JHM855.1.
- 756 NOAA, 2013: Defining El Niño and La Niña. Accessed 2015-
757 08-20, [https://www.climate.gov/news-features/understanding-climate/
758 watching-el-nio-and-la-nia-noaa-adapts-global-warming](https://www.climate.gov/news-features/understanding-climate/watching-el-nio-and-la-nia-noaa-adapts-global-warming).
- 759 O’Gorman, P. A., and T. Schneider, 2009: The physical basis for increases in precipitation ex-
760 tremes in simulations of 21st-century climate change. *Proceedings of the National Academy of
761 Sciences*, **106** (35), 14 773–14 777, doi:10.1073/pnas.0907610106.
- 762 Oleson, K., and Coauthors, 2010: Technical description of version 4.0 of the Community Land
763 Model (CLM). NCAR Technical Note NCAR/TN-478+STR, National Center for Atmospheric
764 Research, Boulder, Colorado, 257 pp. doi:10.5065/D6FB50WZ.
- 765 Pierce, D. W., 2002: The role of sea surface temperatures in interactions between ENSO
766 and the North Pacific Oscillation. *Journal of Climate*, **15** (11), 1295–1308, doi:10.1175/
767 1520-0442(2002)015<1295:TROSST>2.0.CO;2.

- 768 Ralph, F. M., P. J. Neiman, and G. A. Wick, 2004: Satellite and CALJET aircraft observations of
769 atmospheric rivers over the eastern North Pacific Ocean during the winter of 1997/98. *Monthly*
770 *Weather Review*, **132** (7), 1721–1745, doi:10.1175/1520-0493(2004)132<1721:SACAOO>2.0.
771 CO;2.
- 772 Rauscher, S. A., E. Coppola, C. Piani, and F. Giorgi, 2010: Resolution effects on regional climate
773 model simulations of seasonal precipitation over Europe. *Climate dynamics*, **35** (4), 685–711,
774 doi:10.1007/s00382-009-0607-7.
- 775 Rauscher, S. A., T. D. Ringler, W. C. Skamarock, and A. A. Mirin, 2013: Exploring a global
776 multiresolution modeling approach using aquaplanet simulations. *Journal of Climate*, **26** (8),
777 2432–2452, doi:10.1175/JCLI-D-12-00154.1.
- 778 Rhoades, A. M., X. Huang, P. A. Ullrich, and C. M. Zarzycki, 2015: Characterizing Sierra Nevada
779 snowpack using variable-resolution CESM. *Journal of Applied Meteorology and Climatology*,
780 (2015), doi:10.1175/JAMC-D-15-0156.1.
- 781 Rhoades, A. M., P. A. Ullrich, and C. M. Zarzycki, 2016: Projecting 21st century snowpack trends
782 in western USA mountains using variable-resolution CESM. *Climate Dynamics*, under review.
- 783 Riahi, K., and Coauthors, 2011: RCP 8.5 – A scenario of comparatively high greenhouse gas
784 emissions. *Climatic Change*, **109** (1-2), 33–57, doi:10.1007/s10584-011-0149-y.
- 785 Rowell, D. P., and R. G. Jones, 2006: Causes and uncertainty of future summer drying over Europe.
786 *Climate Dynamics*, **27** (2-3), 281–299, doi:10.1007/s00382-006-0125-9.
- 787 Salathé Jr, E. P., R. Steed, C. F. Mass, and P. H. Zahn, 2008: A high-resolution climate model for
788 the US Pacific Northwest: Mesoscale feedbacks and local responses to climate change. *Journal*
789 *of Climate*, **21** (21), 5708–5726, doi:10.1175/2008JCLI2090.1.

- 790 Scoccimarro, E., M. Zampieri, A. Bellucci, A. Navarra, and Coauthors, 2013: Heavy precipitation
791 events in a warmer climate: Results from CMIP5 models. *Journal of Climate*, doi:10.1175/
792 JCLI-D-12-00850.1.
- 793 Seneviratne, S. I., and Coauthors, 2012: Changes in climate extremes and their impacts on the
794 natural physical environment. *Managing the risks of extreme events and disasters to advance
795 climate change adaptation*, 109–230.
- 796 Sillmann, J., V. Kharin, F. Zwiers, X. Zhang, and D. Bronaugh, 2013: Climate extremes indices
797 in the CMIP5 multimodel ensemble: Part 2. Future climate projections. *Journal of Geophysical
798 Research: Atmospheres*, **118** (6), 2473–2493, doi:10.1002/jgrd.50188.
- 799 Simmons, A., K. Willett, P. Jones, P. Thorne, and D. Dee, 2010: Low-frequency variations
800 in surface atmospheric humidity, temperature, and precipitation: Inferences from reanalyses
801 and monthly gridded observational data sets. *Journal of Geophysical Research: Atmospheres*,
802 **115** (D1), doi:10.1029/2009JD012442.
- 803 Singh, D., M. Tsiang, B. Rajaratnam, and N. S. Diffenbaugh, 2013: Precipitation extremes over the
804 continental United States in a transient, high-resolution, ensemble climate model experiment.
805 *Journal of Geophysical Research: Atmospheres*, **118** (13), 7063–7086, doi:10.1002/jgrd.50543.
- 806 Small, R. J., and Coauthors, 2014: A new synoptic scale resolving global climate simulation using
807 the community earth system model. *Journal of Advances in Modeling Earth Systems*, **6** (4),
808 1065–1094, doi:10.1002/2014MS000363.
- 809 Staniforth, A. N., and H. L. Mitchell, 1978: A variable-resolution finite-element technique for
810 regional forecasting with the primitive equations. *Monthly Weather Review*, **106** (4), 439–447,
811 doi:10.1175/1520-0493(1978)106<439:AVRFET>2.0.CO;2.

- 812 Stephens, G. L., and Coauthors, 2010: Dreary state of precipitation in global models. *Journal of*
813 *Geophysical Research: Atmospheres*, **115 (D24)**, doi:10.1029/2010JD014532.
- 814 Stevenson, S., 2012: Significant changes to ENSO strength and impacts in the twenty-first century:
815 Results from CMIP5. *Geophysical Research Letters*, **39 (17)**, doi:10.1029/2012GL052759.
- 816 Sugi, M., and J. Yoshimura, 2004: A mechanism of tropical precipitation change due to
817 CO₂ increase. *Journal of Climate*, **17 (1)**, 238–243, doi:10.1175/1520-0442(2004)017<0238:
818 AMOTPC>2.0.CO;2.
- 819 Taschetto, A. S., A. S. Gupta, N. C. Jourdain, A. Santoso, C. C. Ummenhofer, and M. H. England,
820 2014: Cold tongue and warm pool ENSO events in CMIP5: mean state and future projections.
821 *Journal of Climate*, **27 (8)**, 2861–2885, doi:10.1175/JCLI-D-13-00437.1.
- 822 Taylor, M. A., 2011: Conservation of mass and energy for the moist atmospheric primitive equa-
823 tions on unstructured grids. *Numerical Techniques for Global Atmospheric Models*, Springer,
824 357–380, doi:10.1007/978-3-642-11640-7_12.
- 825 Tebaldi, C., K. Hayhoe, J. M. Arblaster, and G. A. Meehl, 2006: Going to the extremes. *Climatic*
826 *Change*, **79 (3-4)**, 185–211, doi:10.1007/s10584-006-9051-4.
- 827 Trenberth, K. E., 2011: Changes in precipitation with climate change. *Climate Research*, **47 (1)**,
828 123, doi:10.3354/cr00953.
- 829 Trenberth, K. E., A. Dai, R. M. Rasmussen, and D. B. Parsons, 2003: The changing character of
830 precipitation. *Bulletin of the American Meteorological Society*, **84 (9)**, 1205–1217, doi:10.1175/
831 BAMS-84-9-1205.

- 832 Ullrich, P. A., D. Devendran, and H. Johansen, 2016: Arbitrary-order conservative and consistent
833 remapping and a theory of linear maps, part 2. *Monthly Weather Review*, **144** (4), 1529–1549,
834 doi:10.1175/MWR-D-15-0301.1.
- 835 Ullrich, P. A., and M. A. Taylor, 2015: Arbitrary-order conservative and consistent remapping
836 and a theory of linear maps: Part I. *Monthly Weather Review*, **143** (6), 2419–2440, doi:10.1175/
837 MWR-D-14-00343.1.
- 838 Walker, M. D., and N. S. Diffenbaugh, 2009: Evaluation of high-resolution simulations of daily-
839 scale temperature and precipitation over the United States. *Climate Dynamics*, **33** (7-8), 1131–
840 1147, doi:10.1007/s00382-009-0603-y.
- 841 Wehner, M. F., 2013: Very extreme seasonal precipitation in the NARCCAP ensemble:
842 model performance and projections. *Climate Dynamics*, **40** (1-2), 59–80, doi:10.1007/
843 s00382-012-1393-1.
- 844 Wehner, M. F., R. L. Smith, G. Bala, and P. Duffy, 2010: The effect of horizontal resolution
845 on simulation of very extreme US precipitation events in a global atmosphere model. *Climate
846 Dynamics*, **34** (2-3), 241–247, doi:10.1007/s00382-009-0656-y.
- 847 Wehner, M. F., and Coauthors, 2014: The effect of horizontal resolution on simulation quality in
848 the Community Atmospheric Model, CAM5.1. *Journal of Advances in Modeling Earth Systems*,
849 doi:10.1002/2013MS000276.
- 850 Yoon, J.-H., S. S. Wang, R. R. Gillies, B. Kravitz, L. Hipps, and P. J. Rasch, 2015: Increasing
851 water cycle extremes in California and in relation to ENSO cycle under global warming. *Nature
852 Communications*, **6**, doi:10.1038/ncomms9657.

- 853 Zarzycki, C. M., C. Jablonowski, and M. A. Taylor, 2014: Using variable-resolution meshes
854 to model tropical cyclones in the Community Atmosphere Model. *Monthly Weather Review*,
855 **142** (3), 1221–1239, doi:10.1175/MWR-D-13-00179.1.
- 856 Zarzycki, C. M., C. Jablonowski, D. R. Thatcher, and M. A. Taylor, 2015: Effects of localized grid
857 refinement on the general circulation and climatology in the Community Atmosphere Model.
858 *Journal of Climate*, (2015), doi:10.1175/JCLI-D-14-00599.1.
- 859 Zhang, X., L. Alexander, G. C. Hegerl, P. Jones, A. K. Tank, T. C. Peterson, B. Trewin, and
860 F. W. Zwiers, 2011: Indices for monitoring changes in extremes based on daily temperature
861 and precipitation data. *Wiley Interdisciplinary Reviews: Climate Change*, **2** (6), 851–870, doi:
862 10.1002/wcc.147.
- 863 Zhang, X., J. Wang, F. W. Zwiers, and P. Y. Groisman, 2010: The influence of large-scale climate
864 variability on winter maximum daily precipitation over North America. *Journal of Climate*,
865 **23** (11), 2902–2915.

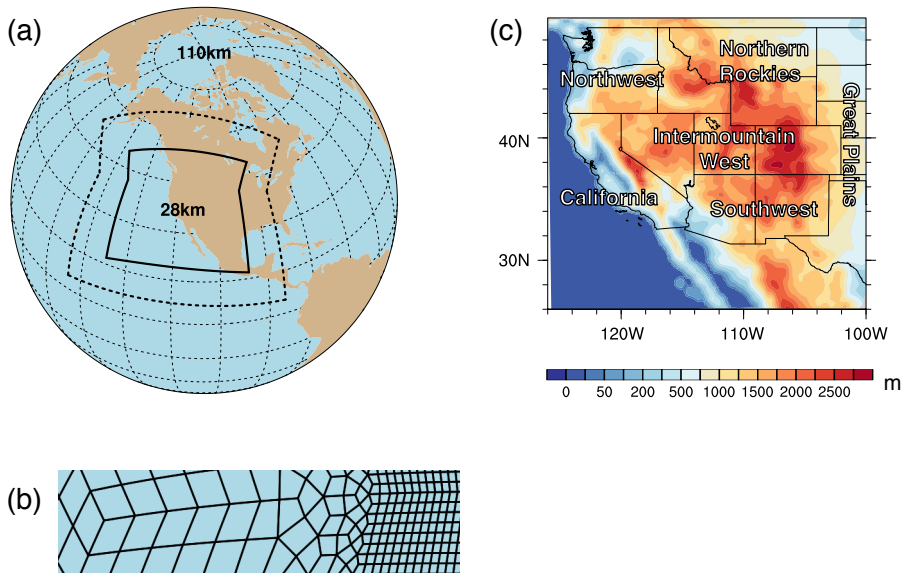
866 LIST OF TABLES

TABLE 1. Precipitation indices employed in this study.

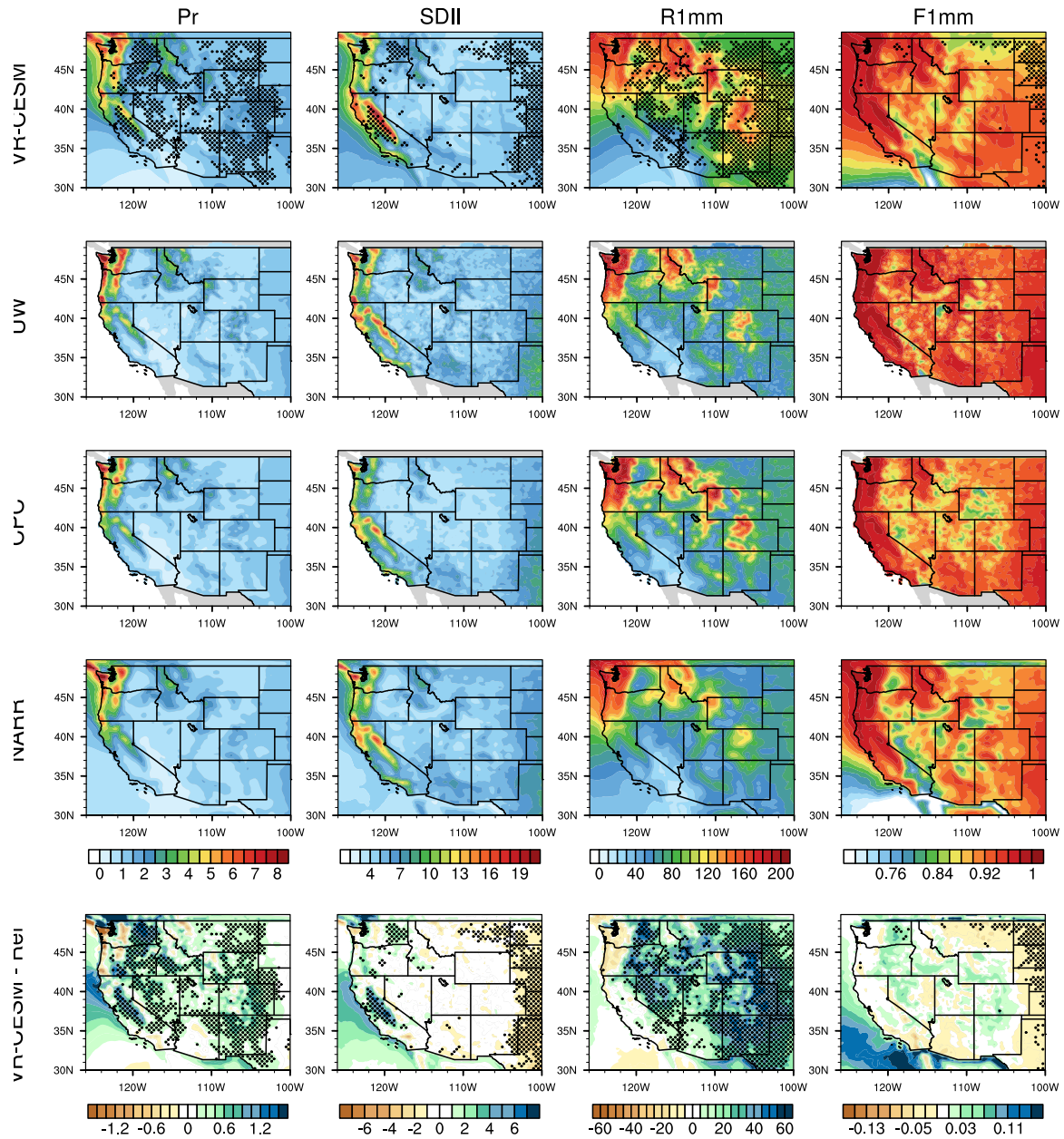
Indice	Definition
Pr	Mean daily precipitation
R1mm	Number of days per year with Pr>1 mm
SDII	Simple precipitation intensity index: Precipitation amount / $\langle R1mm \rangle$ (mm/day)
R5mm	Number of days per year with Pr>1 mm and Pr=<5 mm
R10mm	Number of days per year with Pr>5 mm and Pr=<10 mm
R20mm	Number of days per year with Pr>10 mm and Pr=<20 mm
R40mm	Number of days per year with Pr>20 mm and Pr=<40 mm
Rxmm	Number of days per year with Pr>40 mm
F1mm	Fraction of precipitation contributed to the total precipitation for days of R1mm (similarly for F5mm, F10mm, F20mm, F40mm and Fxmm)
P5mm	Precipitation amount from R5mm (similarly for P10mm, P20mm, F40mm, Pxmm)

868 **LIST OF FIGURES**

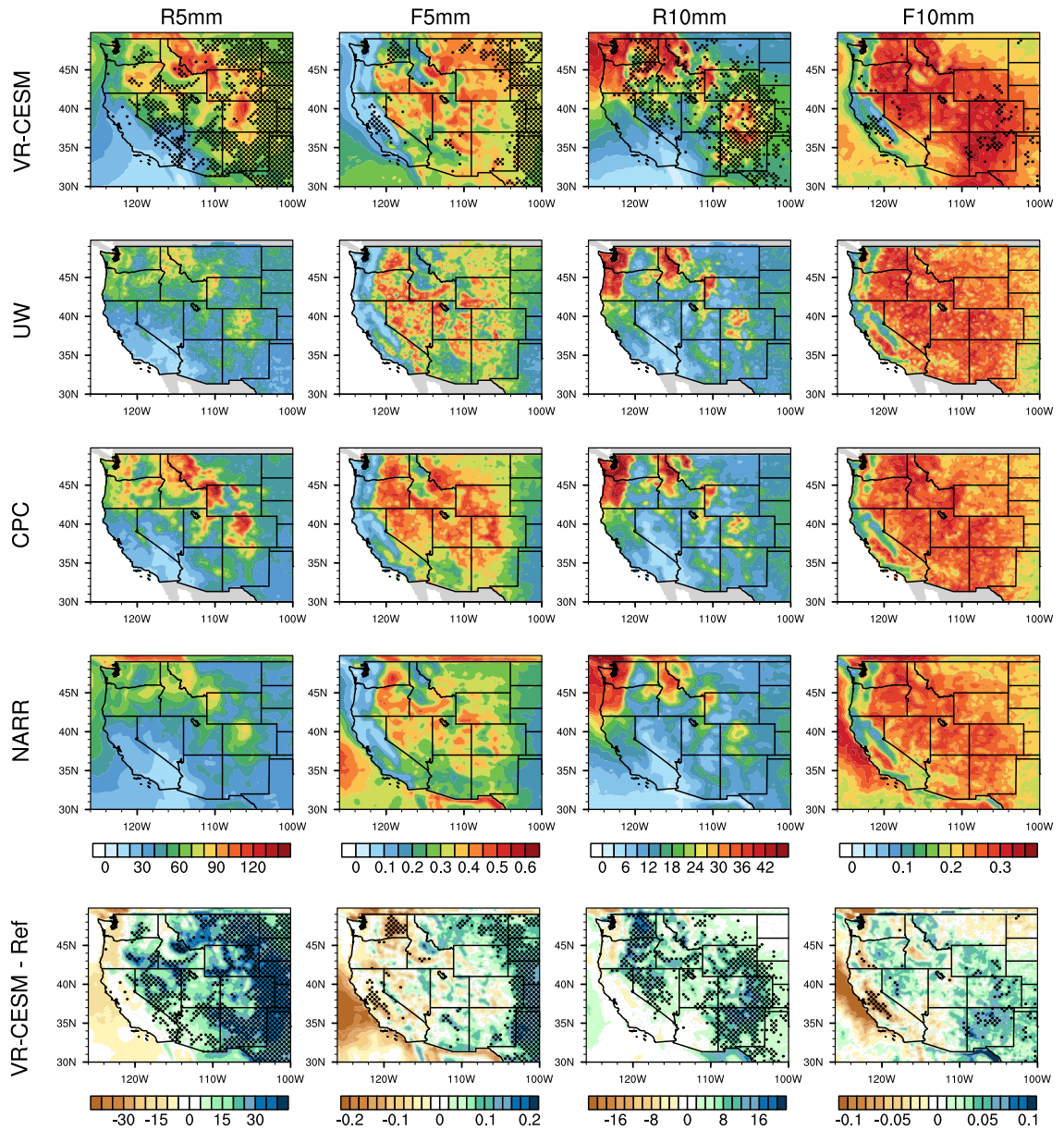
869 Fig. 1.	(a) The approximate grid spacing used for the VR-CESM 0.25° mesh. (b) A depiction of 870 the transition from the global 1° resolution mesh through two layers of refinement to 0.25° . 871 (c) Topography height over the study area.	44
872 Fig. 2.	Mean precipitation and associated indices from VR-CESM and reference datasets over the 873 historical period, 1980-2005. Areas with statistically significance differences are marked 874 with stippling.	45
875 Fig. 3.	Mean precipitation and associated indices from VR-CESM and reference datasets over the 876 historical period, 1980-2005 (continued).	46
877 Fig. 4.	Mean precipitation and associated indices from VR-CESM and reference datasets over the 878 historical period, 1980-2005 (continued).	47
879 Fig. 5.	2m average temperature (Tavg), 2m relative humidity (RH) and mean precipitation (Pr) av- 880 eraged over the historical time period, along with average differences mid-hist and end-hist. 881 Areas with statistically significance differences are marked with stippling.	48
882 Fig. 6.	Differences of precipitation indices Pr (mm/day), SDII and R*mm between hist, mid and 883 end average. Areas with statistically significance differences are marked with stippling.	49
884 Fig. 7.	Differences of precipitation indices Pr (mm/year) and P*mm between hist, mid and end 885 average. Areas with statistically significance differences are marked with stippling. Areas 886 with no data are indicated in gray.	50
887 Fig. 8.	Differences in specific humidity and horizontal wind patterns at 850hPa for moisture flux, 888 and pointwise IVT (averaged over days with (a) $10\text{mm} < \text{Pr} \leq 40\text{mm}$ and (b) $\text{Pr} > 40\text{mm}$) 889 for the cool season (October to March) averaged over 26 years. The minimum wind vector 890 length is set to 0.5 m/s for better visualization. (Lower plot) Specific humidity and wind 891 patterns are averaged over all days over cool season.	51
892 Fig. 9.	Frequency distribution of rainy days ($\text{Pr} \geq 0.1\text{mm/day}$) over the three time periods from 893 all simulations dataset in four regions (with logarithmic vertical scale). (Note: Region (a) 894 to (d) cover Washington and Oregon; California (except northern part, i.e. latitude no larger 895 than 38°); Nevada and Utah; Arizona and New Mexico, respectively.)	52
896 Fig. 10.	Differences of precipitation indices Pr and R*mm between warm and cool phases of ENSO 897 over each time period.	53
898 Fig. 11.	Changes of IVT for simulations under different phases of ENSO of wet season (October to 899 March) over rainy days averaged yearly, with seasonal mean wind patterns at 850hPa (unit: 900 m/s) (Note: The minimum wind vector is set to be 0.5 m/s, therefore, the wind less than 0.5 901 m/s is also plotted at the minimum length for better visualization.)	54



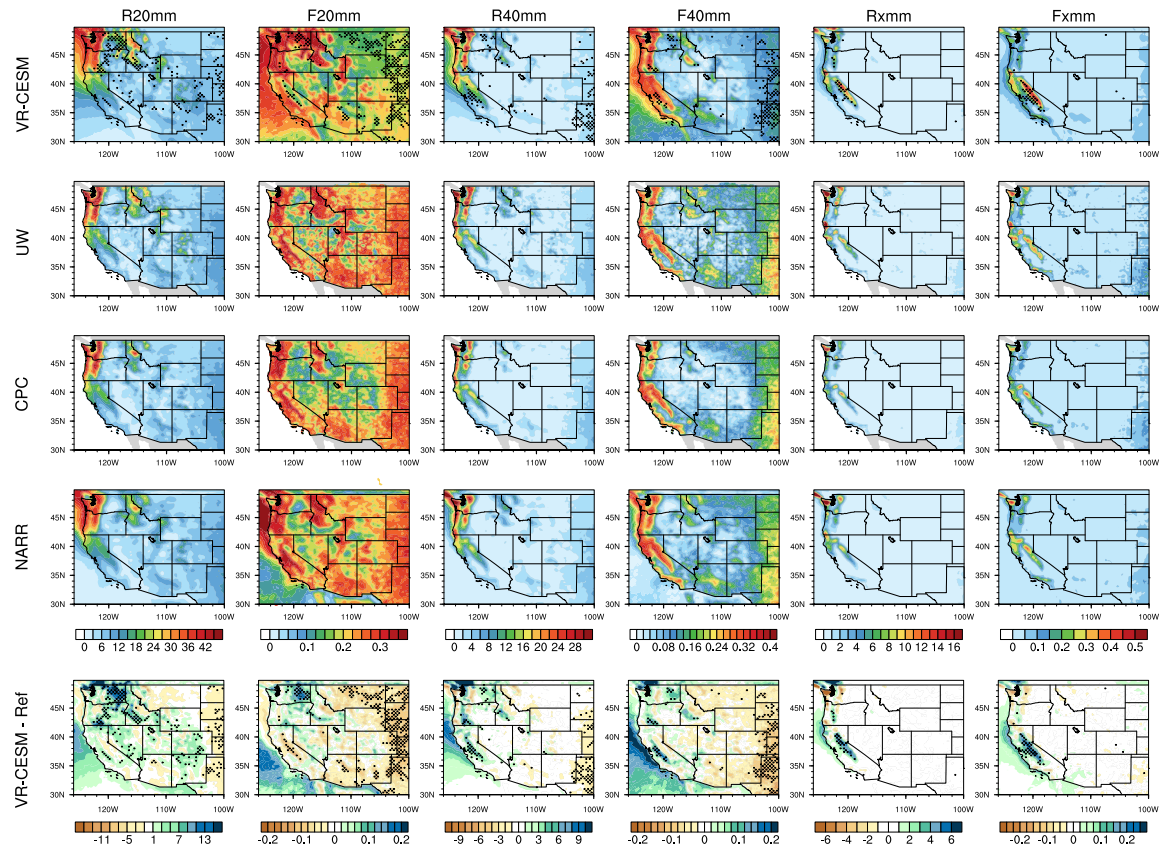
902 FIG. 1. (a) The approximate grid spacing used for the VR-CESM 0.25° mesh. (b) A depiction of the transition
 903 from the global 1° resolution mesh through two layers of refinement to 0.25° . (c) Topography height over the
 904 study area.



905 FIG. 2. Mean precipitation and associated indices from VR-CESM and reference datasets over the historical
906 period, 1980-2005. Areas with statistically significant differences are marked with stippling.



907 FIG. 3. Mean precipitation and associated indices from VR-CESM and reference datasets over the historical
908 period, 1980-2005 (continued).



909 FIG. 4. Mean precipitation and associated indices from VR-CESM and reference datasets over the historical
910 period, 1980-2005 (continued).

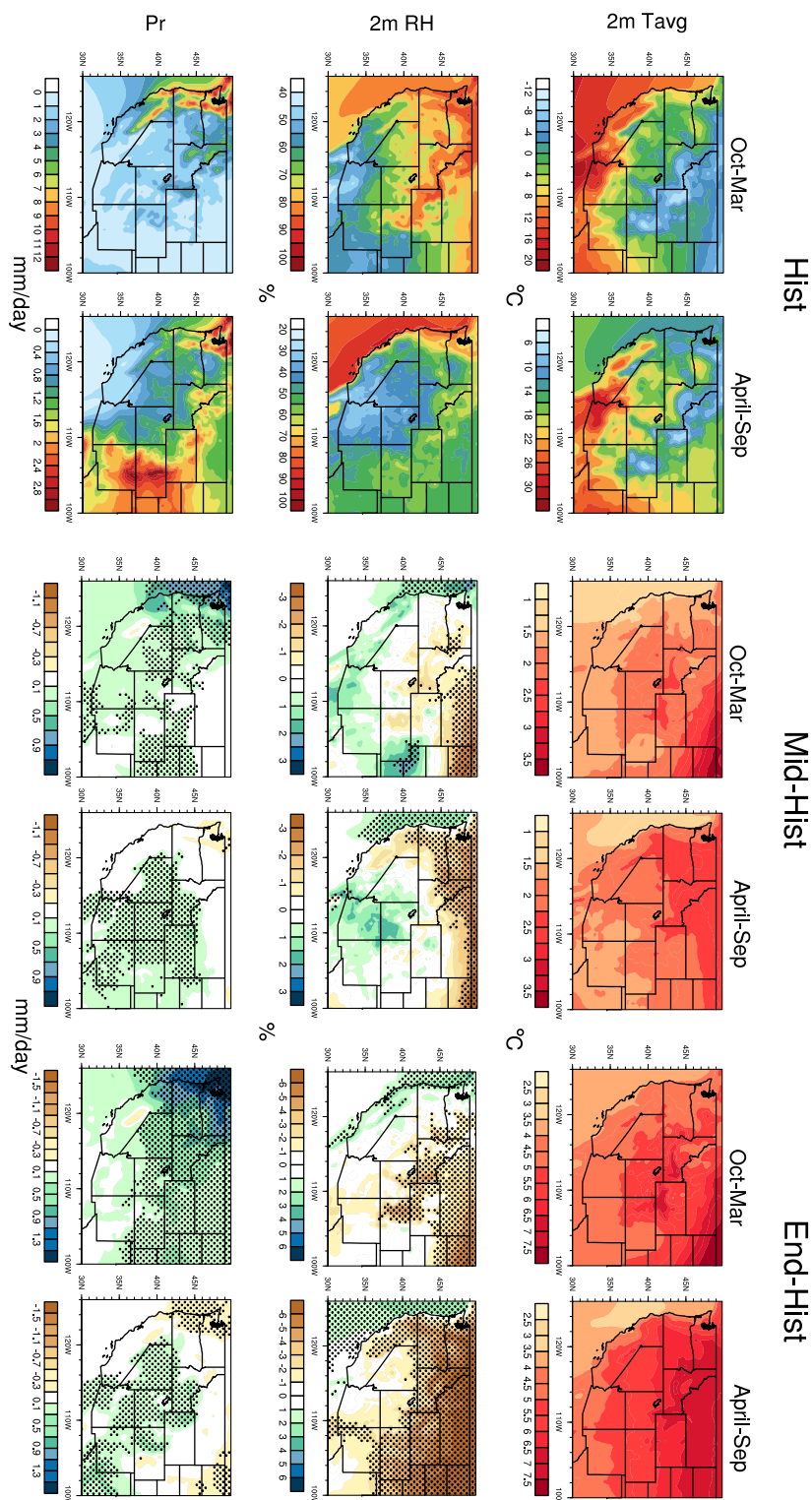
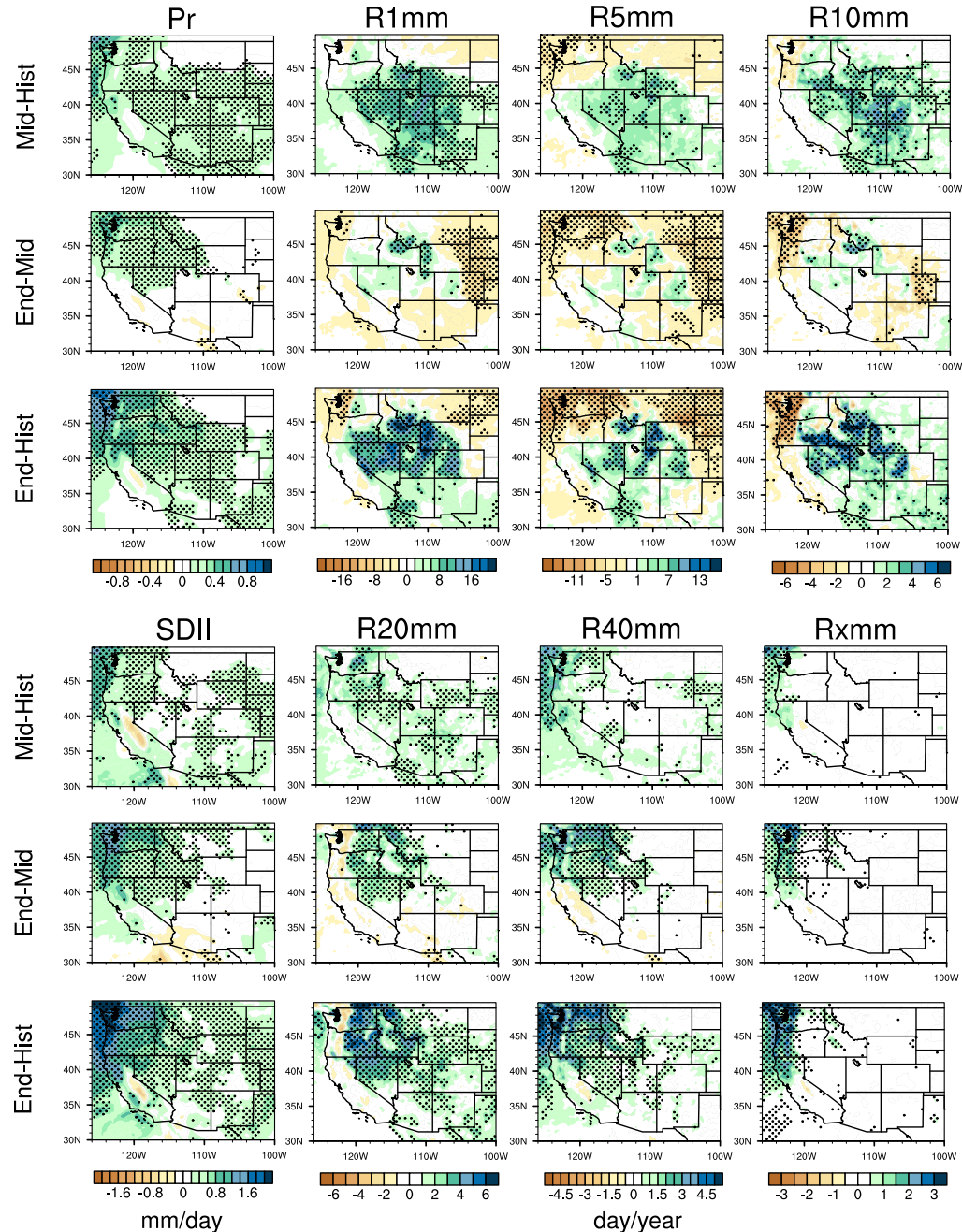


FIG. 5. 2m average temperature (Tavg), 2m relative humidity (RH) and mean precipitation (Pr) averaged over the historical time period, along with
 911
 912 average differences mid-hist and end-hist. Areas with statistically significance differences are marked with stippling.



913 FIG. 6. Differences of precipitation indices Pr (mm/day), SDII and R*mm between hist, mid and end average.

914 Areas with statistically significant differences are marked with stippling.

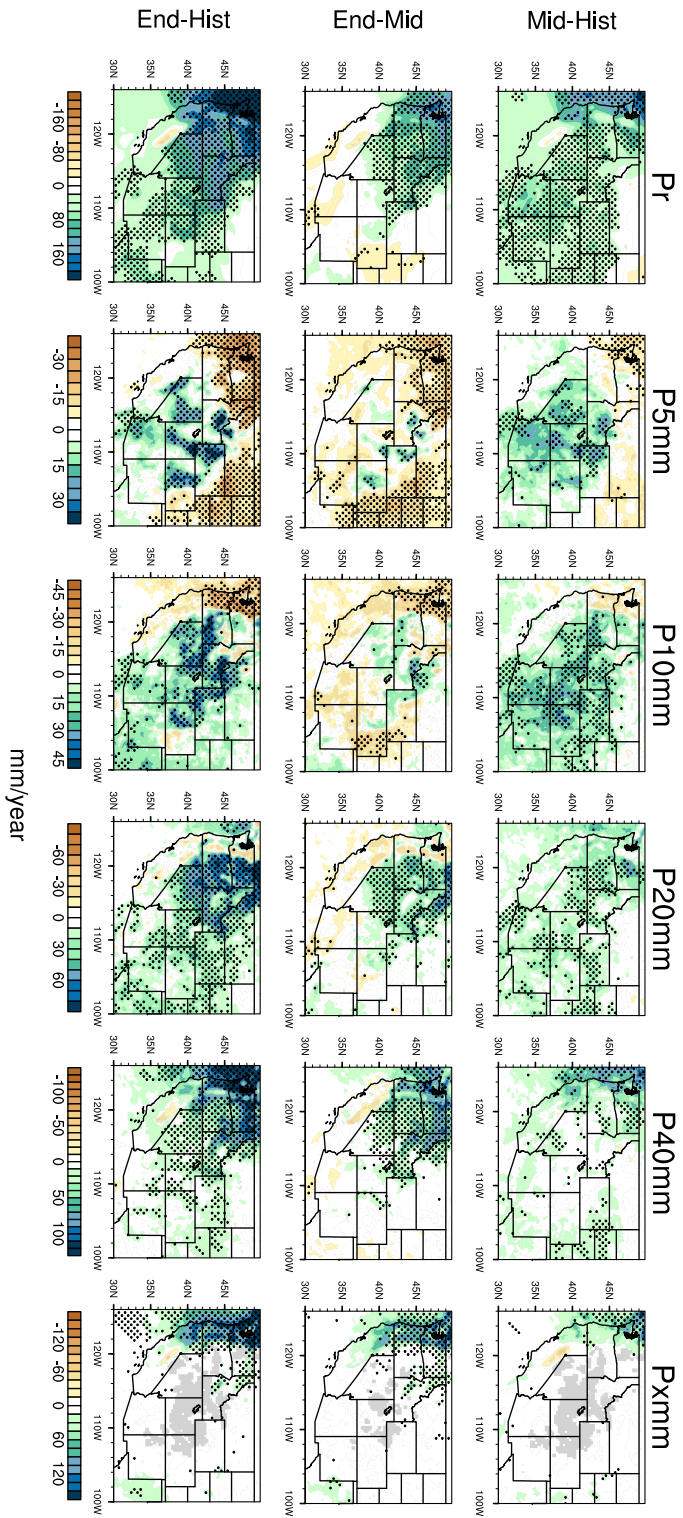
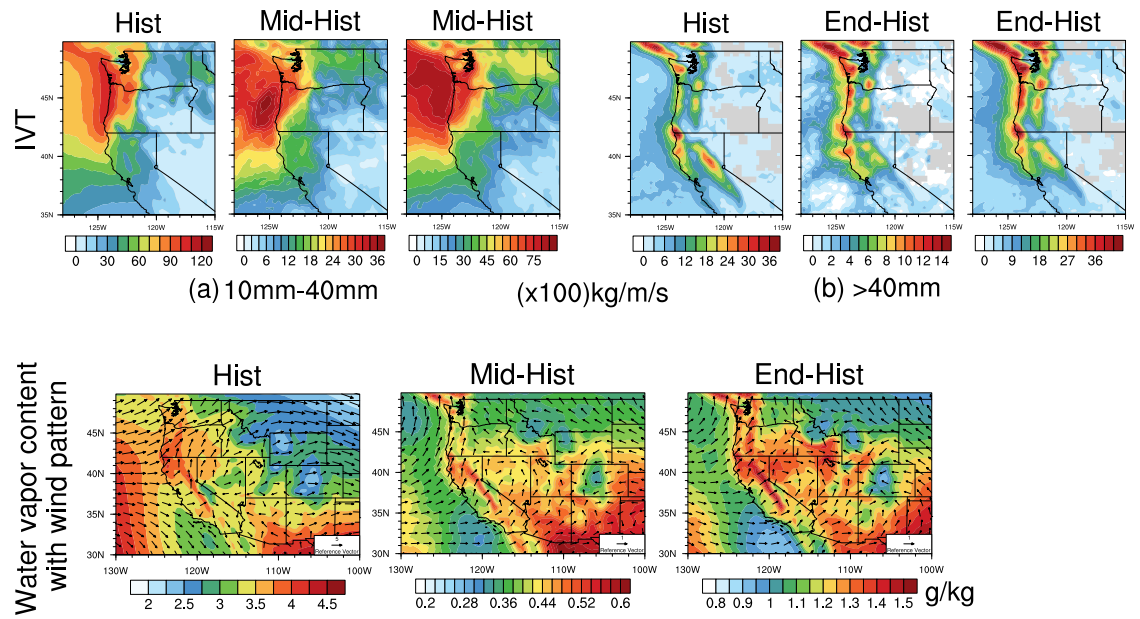


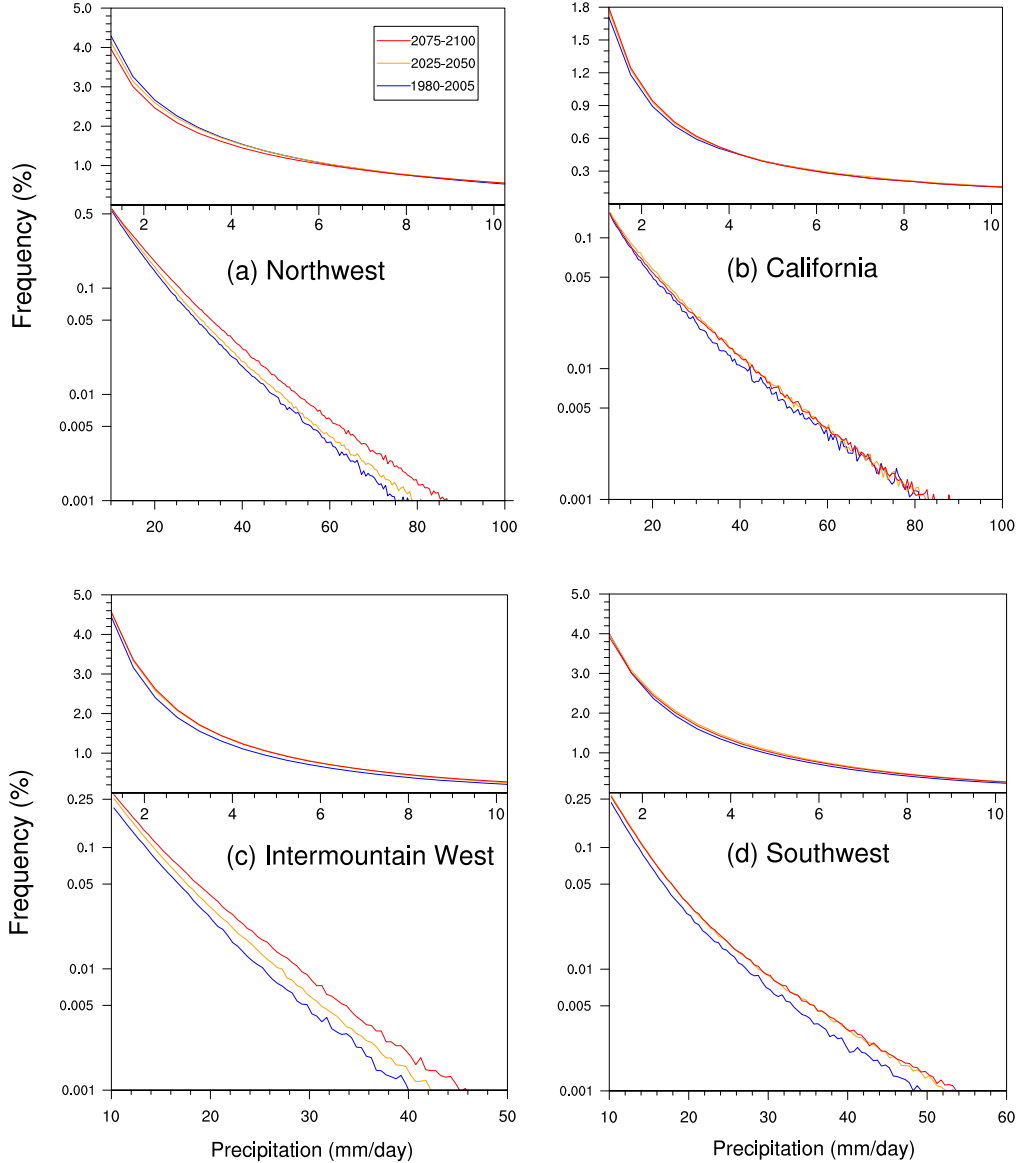
FIG. 7. Differences of precipitation indices Pr (mm/year) and P_{*mm} between hist, mid and end average. Areas with statistically significance differences are marked with stippling. Areas with no data are indicated in gray.

915

916



917 FIG. 8. Differences in specific humidity and horizontal wind patterns at 850hPa for moisture flux, and point-
 918 wise IVT (averaged over days with (a) $10\text{mm} < \text{Pr} \leq 40\text{mm}$ and (b) $\text{Pr} > 40\text{mm}$) for the cool season (October
 919 to March) averaged over 26 years. The minimum wind vector length is set to 0.5 m/s for better visualization.
 920 (Lower plot) Specific humidity and wind patterns are averaged over all days over cool season.



921 FIG. 9. Frequency distribution of rainy days ($\text{Pr} \geq 0.1\text{mm/day}$) over the three time periods from all simu-
 922 lations dataset in four regions (with logarithmic vertical scale). (Note: Region (a) to (d) cover Washington and
 923 Oregon; California (except northern part, i.e. latitude no larger than 38°); Nevada and Utah; Arizona and New
 924 Mexico, respectively.)

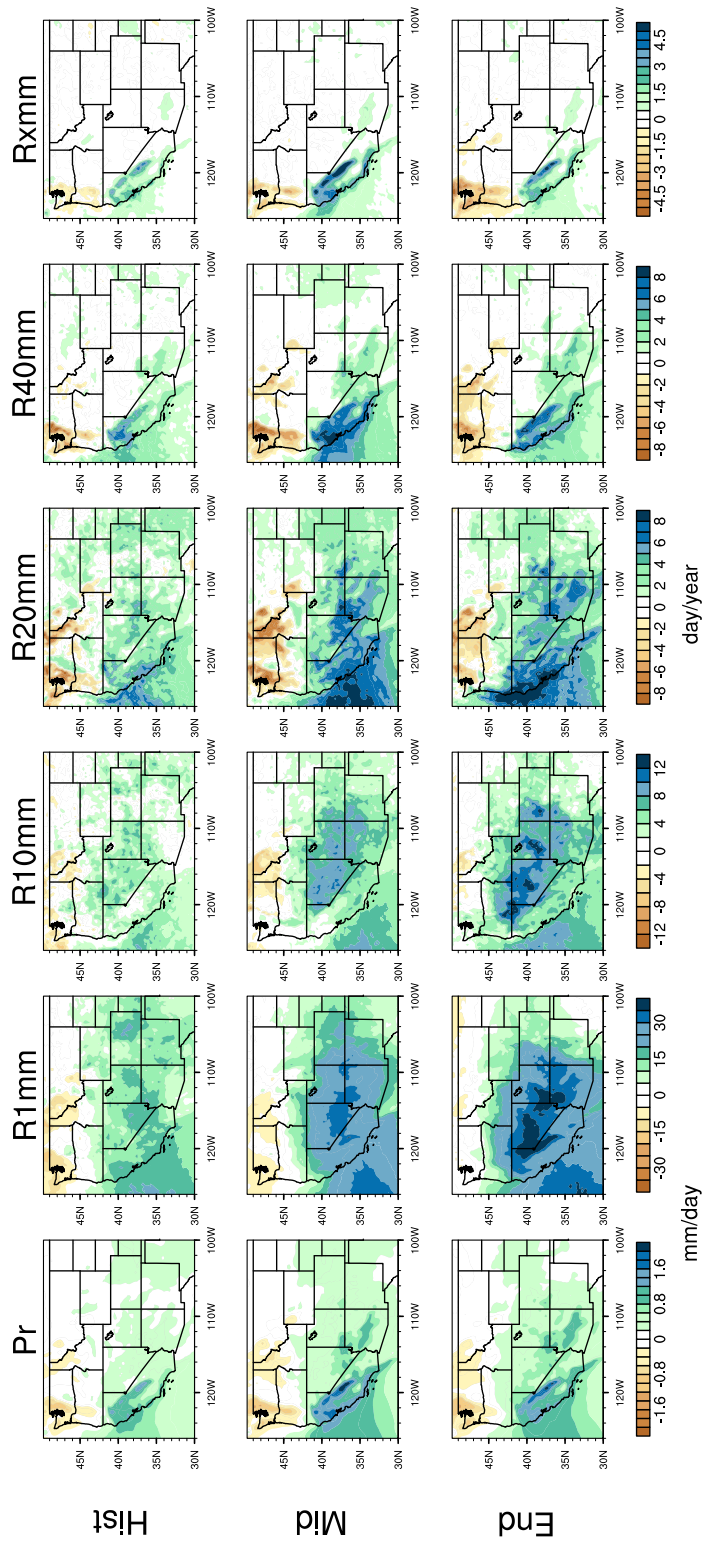
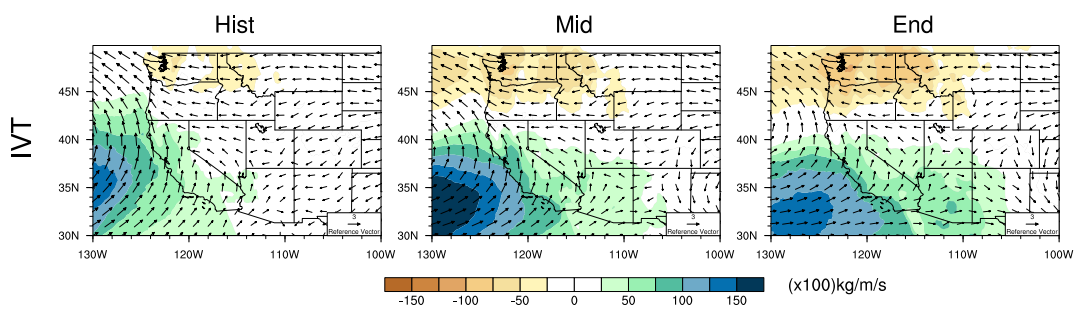


FIG. 10. Differences of precipitation indices Pr and $R_{\ast}mm$ between warm and cool phases of ENSO over each time period.



925 FIG. 11. Changes of IVT for simulations under different phases of ENSO of wet season (October to March)
926 over rainy days averaged yearly, with seasonal mean wind patterns at 850hPa (unit: m/s) (Note: The minimum
927 wind vector is set to be 0.5 m/s, therefore, the wind less than 0.5 m/s is also plotted at the minimum length for
928 better visualization.)